A Study on the Fatigue Assessment of Offshore Steel Catenary Riser

by

Eileen Wong Wee Chin

16117

Dissertation submitted in partial fulfilment of

the requirements for the

Bachelor of Engineering (Hons)

Mechanical Engineering

JANUARY 2016

Universiti Teknologi PETRONAS
Bandar Seri Iskandar
31750 Tronoh
Perak Darul Ridzuan

CERTIFICATION OF APPROVAL

A Study on the Fatigue Assessment of Offshore Steel Catenary Riser

by

Eileen Wong Wee Chin

16117

A project dissertation submitted to the
Mechanical Engineering Programme
Universiti Teknologi PETRONAS
in partial fulfilment of the requirements for the
Bachelor of Engineering (Hons)
Mechanical Engineering

Approved by,

_____
(AP DR. FAKHRULDIN MOHD HASHIM)

UNIVERSITI TEKNOLOGI PETRONAS
TRONOH PERAK
January 2016

CERTIFICATION OF ORIGINALITY

This is to certify that I am responsible for the work submitted in this project, that the original work is my own except as specified in the references and acknowledgements, and that the original work contained herein have not been undertaken or done by unspecified sources or persons.

_____

EILEEN WONG WEE CHIN

ABSTRACT

Declination of production from onshore and shallow water reserves has fostered the deepwater field development. Safe and robust designs of structures and systems for deepwater offshore development are relatively complicated due to the impact of high current and wave. Hence, investigation of the fatigue performance of steel catenary riser (SCR) in associated with vortex-induced vibration (VIV) is relatively important, considering VIV is one of the important factors causing fatigue damage of deepwater SCR. The lack of comprehensive studies of the effect of current profiles to the VIV fatigue damage of SCR prompts the investigation of VIV fatigue performance of SCR in this study. This study aims to propose a new approach that utilises current index concept and Fatigue Damage-Current Index (FD-CI) diagram to establish the relationship between current profiles and VIV short term fatigue damage of SCR for fatigue damage estimation. In this study, statistical model of current profile variation with depth is developed. Current index is proposed as a characteristic value that describes the uniqueness and parameters of each current profile. 46 current profile scenarios are applied to determine the influence of current load in estimation of short-term VIV fatigue damage and FD-CI diagrams were established. The results show fatigue damage rate increases proportionally with velocity raised to the power of 4.4. This relationship can be expressed in form of current index and FD-CI diagrams and defined using empirical equation, such that maximum fatigue damage is expressed as polynomial function of current index. The comparison of result using current index concept with the computational result in SHEAR7 shows that the proposed approach is more conservative in estimating fatigue damage of SCR, but also proves the potential application of current index concept in predicting fatigue damage of SCR for screening purpose in preliminary design stage in a field development.

ACKNOWLEDGEMENTS

First and foremost, author would like to express my utmost gratitude to my supervisor, AP Dr. Fakhruldin Mohd Hashim for the guidance and help throughout the process of performing the research and preparing reports and presentation. His useful advices and comments helps to improve the quality of the project and enhance my report-writing skill.

Secondly, author also like to express my deepest appreciation to my co-supervisor, Dr Kim Do Kyun for his consistent guidance and support in helping author to complete the project smoothly and his sharing of advices to improve the overall presentation of project work. Author would like to express deepest thanks to Professor Choi Han Suk in POSTECH for teaching me the knowledge and understanding of offshore pipeline and riser and providing me the authority to use the software for conducting the simulation and computational work. Besides that, author would like to express my gratitude to examiner, Dr Mark Ovinis for his feedback and comments for the betterment of this project.

Next, author would to like to thank Mr Shin Chul Soon and Mr Ahn Eui Ree for their help in teaching author in using the software and sharing their ideas for the research and knowledge regarding pipeline and riser. A big thank to all the friends and family for giving me support and spirit to complete this project.

TABLE OF CONTENTS

CERTIFICATION OF APPROVAL ..... **i**
CERTIFICATION OF ORIGINALITY ..... **ii**
ABSTRACT ..... **iii**
ACKNOWLEDGEMENTS ..... **iv**
LIST OF FIGURES ..... **vi**
LIST OF TABLES ..... **viii**
ABBREVIATIONS ix
NOMENCLATURES ..... **x**
CHAPTER 1: INTRODUCTION **1**
1.1 Background 1
1.2 Problem Statement 2
1.3 Objectives 3
1.4 Scope of Study 4
CHAPTER 2: LITERATURE REVIEW **5**
2.1 Overview 5
2.2 Review of Vortex Induced Vibration (VIV) 5
2.3 VIV Assessment Approaches 6
2.4 VIV Fatigue Analysis of SCR 7
CHAPTER 3: METHODOLOGY/ PROJECT WORK **8**
3.1 Research Methodology 8
CHAPTER 4: GENERATION OF CURRENT PROFILE MODEL **11**
4.1 Compilation of Current Data 11
4.2 Generation of Current Profile Model by Statistical Mean 12
4.3 Results 13
CHAPTER 5: DEVELOPMENT OF CURRENT INDEX AND FD-CI DIAGRAM **16**
5.1 Modelling of SCR 16
5.2 Analysis of VIV Fatigue Damage of SCR for Selected Current Profile Scenarios 18
5.3 Results 24
5.4 Discussions 31
CHAPTER 6: CONCLUSION AND RECOMMENDATION **40**
REFERENCES **42**

APPENDICES **45**
APPENDIX A: SCR model input data 45
APPENDIX B: Gantt Chart and Milestones 48
APPENDIX C: Best Fit Probability Density Distribution for Each Normalized Water Depth..... 50

LIST OF FIGURES

FIGURE 3.1: General procedure of analysis 8
FIGURE 4.1: Compilation of current profile energy (BP, 2015) 11
FIGURE 4.2: Probability density of actual current velocity along normalised depth13
FIGURE 4.3: Relationship of location parameter with normalized water depth.....14
FIGURE 4.4: Relationship of scale parameter with normalized water depth.....14
FIGURE 4.5: Current profile model along normalized water depth using approximate probability density distribution 15
FIGURE 5.1: SCR model in OrcaFlex.....16
FIGURE 5.2: SCR model with section definition.....17
FIGURE 5.3: Representative current profile for different regions 18
FIGURE 5.4: Definition of current profile shape and parameter.....19
FIGURE 5.5: Individual current profile scenarios.....20
FIGURE 5.6: Motion of riser with respect to current heading direction 23
FIGURE 5.7: Fatigue damage rate along whole riser.....20
FIGURE 5.8: Maximum fatigue damage versus current velocity.....23
FIGURE 5.9: Modal power versus mode number for all scenarios.....26
FIGURE 5.10: Maximum fatigue damage for all 46 current profile scenarios 28
FIGURE 5.11: Maximum fatigue damage location for all 46 current profile scenarios.....28
FIGURE 5.12: VIV fatigue damage result for scenario 25 to 29.....29
FIGURE 5.13: Fatigue damage rate along whole riser for scenario 41 to 43.....30
FIGURE 5.14: Fatigue damage rate along whole riser for scenario 56 to 59.....31
FIGURE 5.15: Fatigue Damage - Current Index (FD-CI) diagram at 0 degree current heading direction (Near case).....34

FIGURE 5.16: Fatigue Damage - Current Index (FD-CI) diagram at 180 degree current heading direction (Far case)....34
FIGURE 5.17: Comparison of fatigue damage for 0 and 180 degree current heading directions....35
FIGURE 5.18: Flowchart of proposed approach for estimating short-term VIV fatigue damage using current index concept.....36
FIGURE 5.19: Comparison of maximum fatigue damage using proposed approach and SHEAR7 software for near case....37
FIGURE 5.20: Comparison of maximum fatigue damage using proposed approach and SHEAR7 software for far case....38
FIGURE B.1: Gantt chart for Final Year Project 1....48
FIGURE B.2: Gantt chart for Final Year Project 2....48
FIGURE C.1: Best fit probability density distribution for each normalized water depth....50
FIGURE C.2: Best fit probability density distribution for each normalized water depth....51
FIGURE C.3: Best fit probability density distribution for each normalized water depth....52
FIGURE C.4: Best fit probability density distribution for each normalized water depth....53
FIGURE C.5: Best fit probability density distribution for each normalized water depth....54
FIGURE C.6: Best fit probability density distribution for each normalized water depth....55
FIGURE C.7: Best fit probability density distribution for each normalized water depth....56

LIST OF TABLES

TABLE 5.1: Current parameters for all 46 current profile scenarios 21
TABLE 5.2: Current index value (CI) for all 46 current profile scenarios.....33
TABLE 5.3: Comparison of maximum fatigue damage computed using proposed approach using CI concept and using industrial software, SHEAR7.....37
TABLE A1: SCR pipe structural data.....45
TABLE A2: Internal fluid data 45
TABLE A3: SCR Tapered stress joint properties.....46
TABLE A4: SCR Strake properties.....46
TABLE A5: Associated wave and wind data 47
TABLE A6: Soil friction coefficient and stiffness 47
TABLE A7: S-N curve parameter.....47

ABBREVIATIONS

API	American Petroleum Institute
CF	Cross flow
CFD	Computational fluid dynamic
CI	Current index
DNV	DET NORSKE VERITAS
GOM	Gulf of Mexico
HVIV	Vortex-induced hull heave motion
IL	In-line
OD	Outer diameter
POSTECH	Pohang University of Science and Technology
Pre-FEED	Pre-Front End Engineering and Design
RMS	Root-mean squared
SCR	Steel catenary riser
TSJ	Tapered stress joint
TTR	Top-tensioned riser
UTP	Universiti Teknologi PETRONAS
VIM	Vortex-induced hull motion
VIV	Vortex-induced vibration
WIM	Wave-induced vibration
WT	Wall thickness

NOMENCLATURES

m_t	Mass per unit length including the added mass
$C_L(\mathrm{x};\omega_r)$	Lift coefficient of mode r
$\ddot{y}$	Acceleration of the structure
$\dot{y}$	Velocity of the structure
ρ_f	Fluid volume density
$\Delta\sigma$	Hot spot nominal stress range
a	Intercept on cycle axis for S-N curve
b	Slope of S-N curve
N	Number of cycle to failure
r	Mode number
V	Current velocity along the water depth
α	Region coefficient
CI	Current index
D	Diameter of the cylinder
$P(x,t)$	Lift force per unit length
R	Damping per unit length including strutural and hydrodynamic damping
T	Tension
$V(x)$	Velocity of flow
t	Temporal variable
x	Spatial variable
x/d	Normalized water depth
$y"$	Second derivative of the displacement of the structure with respect to spatial variable
μ	Location parameter
σ	Scale parameter
ω	Frequency of structure

CHAPTER 1

INTRODUCTION

1.1 Background

With the depletion of onshore and shallow water reserves, oil and gas field development has been shifted to deepwater regions progressively over the last few decades to meet the growing worldwide energy demands. The harsh and unpredictable environmental conditions in deepwater region have caused the increase in complexity in designing a functional and robust offshore structure. Riser system, as an integral element of the offshore structure, plays an important role to ensure safe transport of hydrocarbon from the wellhead at the seabed to the platform, as well as transport of processed fluid from platform to subsequent storage unit or onshore facility.

Various types and configurations of riser systems have been developed to fit different operational purposes and to adapt to different ocean conditions in field developments [1]. Of all riser systems, steel catenary riser (SCR) is the most promising solution for deepwater development due to its lower construction cost, ease of fabrication, ability to sustain high pressure and high temperature condition and good adaptability to drift and heave motion of platform [2]. SCR is a proven technology along with 22 years of history. The first SCRs were installed on Shell's Auger TLP for oil and gas export in the Gulf of Mexico [3].

SCR is a steel riser without intermediate buoys or floating devices that is suspended from the platform, forming a catenary shape with bottom end laying along the seabed [4]. The configuration and characteristic of SCR have caused it to be sensitive to environmental loads such as wave, wind and current, along with the soil condition of the seabed. One of the important issues that is considered in design and analysis phase is the fatigue damage suffered by SCR over its period of operating in deepwater region. There are several factors contributing to fatigue damage of SCRs, mainly waves induced hull motions (WIM), vortex-induced vibrations (VIV), vortex-induced hull motion (VIM), hull heave induced VIV (HVIV) and installation works. VIV is considered the most critical factor in designing SCRs, especially for deepwater SCRs that operate in high current regions. The riser vibrates at high frequency due to the

vortex shedding leading to higher frequency of cyclic stress, resulting in higher rate of fatigue damage. Several VIV mitigation methods are proposed and implemented to reduce VIV or prevent formation of vortices, including installation of VIV suppression device such as fairing and strakes [1].

1.2 Problem Statement

To design a technically feasible and economically viable deepwater SCR, analyzing the fatigue performance of SCR is the vital part in the design process. SCR is susceptible to fatigue damage due to high cyclic stress imposed by the environmental loads. Current load appears to be highly perilous to riser because when fluid flows around the circular cylinder, vortex shedding occurs which causes pressure differential around the cylinder and induces forces on the cylinder, causing it to vibrate. This vibration is generally known as vortex-induced vibration. When the cylinder vibrates at or near to the frequency of vortex shedding, lock-in phenomenon happens, which excites very high response amplitude of vibration of the riser and causes the fatigue failure of the riser structure [5]. The riser failure may lead to release of hydrocarbon and production shutdown and eventually pollution which is detrimental to public safety, economic and environment. Many studies regarding VIV response of cylindrical structure have hitherto been performed, yet the understanding of VIV response of deepwater riser is insufficient with great amount of uncertainty due to the lack of understanding of performance of SCR at high Reynolds number regime. This shows the need to conduct an in-depth investigation of VIV fatigue performance of a deepwater SCR.

Semi empirical models and computational fluid dynamics (CFD) simulations have been developed to predict VIV response and the corresponding fatigue damage of a riser system. Several state-of-practice software such as SHEAR7, VIVA and VIVANA are widely employed in industry to analyze the fatigue performance of the riser. However, estimating fatigue damage using these existing semi empirical tools has been proven to be difficult with estimated results considerably different from measured data due to limitation of model test data [6]. Analysis using 2D CFD, which is based on simplified assumptions of the fluid flow field and response characteristics, does not

represent the actual three dimensional flow around the cylinder. Yet, 3D CFD simulation that provides better accuracy demands a great amount of computational time [7], [8]. Hence, an easy and efficient method to estimate the fatigue damage of riser using field data as the input is veritably required.

In addition, VIV is implied to be more sensitive to current profile in terms of its magnitude and shape variation with the water depth than to other parameters [1], [9]. Gao et al. [10] also addressed the dependence of VIV fatigue damage of SCR on the current profile. However, the understanding of the effect of current composed of varying velocity along the water depth on the SCR in association with VIV remains deficient. Undeniably, an extensive analysis of fatigue damage with respect to current loads in conjunction with VIV is essential. In this study, fatigue damage versus current index (FD-CI) diagram is proposed to establish the relationship between current profile and VIV fatigue performance of SCR.

1.3 Objectives

The primary objective of this study is to propose a new approach to estimate the short-term fatigue damage of SCR caused by VIV. In order to arrive at this primary objective, the following sub-project deliverables are to be pursued. These are:

- To develop statistical model of current profile variation with depth using probability density distribution.

- To develop current index equation that can describe characteristic of each current profile.

- To establish the relationship between the current profile and short-term VIV fatigue performance of SCR using Fatigue Damage-Current Index (FD-CI) Diagram

1.4 Scope of Study

The main emphasis of this study is short-term fatigue damage due to VIV experienced by SCR. The VIV fatigue analysis is conducted on a SCR model constructed based on an imaginary environment created with the assumption such that the riser is installed in Gulf of Mexico (GOM). Semi empirical tool, OrcaFlex, is used to build the model and to run analysis. SHEAR7 is used in conjunction with OrcaFlex to compute the total fatigue damage of SCR caused by VIV. The design of the SCR model is in accordance with the design codes and standards from API and DNV. Fatigue damage due to other factors such as VIM, VIV, HVIV and installation is not within the concern of this study.

Study is performed to investigate the effect of variation of current profile parameter only. Of particular relevance is the current magnitude and shape to the VIV response of the SCR. Variation of wave and wind data will not be taken into consideration in this study and thus, these data will be fixed for all scenarios. The current is assumed to be unidirectional throughout the water depth. The analysis will be performed for two current heading directions, namely near and far cases.

CHAPTER 2

LITERATURE REVIEW

This chapter summarizes and reviews previous literatures relevant to VIV and fatigue damage of SCR. A general overview of fatigue damage of SCR is provided, followed by description of VIV, assessment methods and studies of VIV fatigue analysis of SCR.

2.1 Overview

In the process of designing a SCR, fatigue is one of the key issues to be scrutinized and tackled. Campbell [11] made a remark upon the complexity of fatigue analysis of a riser system due to consideration of combination of several factors that contribute to accumulation of fatigue damage in long term, including first order loading, low frequency second order vessel motion, vessel springing and VIV. Among all, VIV is the most inimical to the fatigue failure of bare SCR, particularly in deepwater region with severe current, where the ocean current is expected to give rise to VIV that can lead to fatigue damage which has detrimental effects in term of safety and expenses of riser system [4], [12].

2.2 Review of Vortex-Induced Vibration (VIV)

To comprehend the impact of VIV to SCR, the phenomenon of VIV has to be examined thoroughly. The VIV response of a cylindrical structure has been studied intensively over the past few decades. It is commonly understood as the vibration caused by vortex shedding that produces alternating forces on the cylinder [13], [14]. Commensurate with similarity in the fluid flow characteristics surrounding the cylinder, Lienhard [15] categorized flow regimes into several Reynolds number ranges. He developed the relationship between Strouhal number and Reynolds number for circular cylinder which is generally used to determine vortex shedding frequency causing VIV. His finding is being referred by many scholars in latter studies. Vandiver [16] indicated the strong effect of mass ratio in such the way that low mass ratio cylinder will have a broader lock-in range. In latter year, Vandiver et al. [17] proposed the usage of shear parameter and number of potentially responding modes to predict the possibility of occurrence of lock-in phenomenon. A comprehensive review of

fundamental discoveries with respect to VIV can be found in Williamson and Govardhan [18].

2.3 VIV Assessment Approaches

To study the effect of VIV to riser, VIV analysis is normally performed using numerical models or through experimental investigation. Numerous semi-empirical or empirical methods and tools have been developed based on different approaches, such as SHEAR7 [19], VIVANA [20] and VIVA [21]. SHEAR7 is the most commonly used software in industry. Besides empirical methods, a number of researchers utilized computational fluid dynamics (CFD) simulation to analyse riser response to VIV. Strip theory is commonly used where fluid flow solutions represented in term of strips are computed on series of two-dimensional (2D) planes distributed over the riser length and combined with riser structural model [22], [23]. However, its inability to reproduce the actual three-dimensional (3D) flow and certain geometries was pinpointed by Holmes et al. [7]. To overcome these shortcomings, they simulated VIV response using 3D CFD. Huang [24] also conducted 3D CFD time domain simulation of VIV using Finite-Analytic Navier-Stokes (FANS) code. The good agreement of the result with previous published experimental data suggested the validity of using 3D CFD for VIV simulation. Additional works need to be performed to verify the accuracy of 3D CFD analysis of VIV response of riser.

In the investigation of the accuracy of numerical models in estimating VIV of a riser, Chaplin et al. [25] compared the predictions of 11 numerical models with the laboratory test measurement. They deduced empirical models to be more accurate in predicting cross flow displacements and curvatures than CFD simulation. Despite the popular usage of numerical models in industry for designing riser, Lim and Howells [12] criticised the unreliability of the analytical methods in assessing deepwater riser VIV response due to the fact that these analytical tools are developed using small scale tests with low Reynolds number which are substantially different from real-life riser and current condition. They emphasized the need to conduct in-service monitoring and full scale testing for better prediction of VIV response. Trim et al. [6] also highlighted the inconsistency of calculated marine riser vortex-induced vibration (VIV) fatigue damage using computer model with the observed measurement of VIV-related damage.

Thus, it is recommended that calibration of analytical tool to be done from time to time with updated data acquired from testing or in-field monitoring.

2.4 VIV Fatigue Analysis of SCR

Most of the understanding of VIV is based on straight riser model, flexible riser and simple cylindrical structure, which is distinct from SCR that has catenary shape and free hanging characteristic. More studies have been performed in recent years on SCR which reveals some significant VIV behaviour of the SCR. Srinil et al. [26] presented a reduced-order model based on geometrically equations of 3D motion of pinned-pinned tensioned-beam or flexural cable that is capable of analysing VIV of catenary riser in ocean current. Gao et al. [27] adopted a simplified vibration model with the characteristics of SCR and found that maximum fatigue damage increases as current velocity increases. In the following year, Gao et al. [10] applied modal superposition method to determine VIV fatigue damage in SCR modelled using a simplified pinned-pinned cable. They discovered the close relation between VIV fatigue damage of the riser and the current profile, in the sense that the number of modes which contribute to vibration of the riser increases when current velocity increases. They also ascertained section close to touchdown zone usually has the maximum fatigue damage.

Lejlic [28] further investigated on the distribution of accumulated fatigue damage of SCR near touchdown point by making probability distribution of mean floater position to calculate VIV fatigue using data from Det Norske Veritas (DNV). Quéau et al. [29] developed method to estimate critical stress range in touchdown zone for sensitivity studies from the examination of 57023 configurations of SCR under static loading. High vessel motion, submerged weight, soil stiffness, low outside diameter over wall thickness ratio, pipeline tension and water depth were found to be damaging to fatigue life of SCR in the touchdown zone. Sun et al. [30] further justified that point close to top end of riser is vulnerable to fatigue damage mainly due to cross-flow vibration whereas the touchdown point has high stress ascribed to in-line VIV. Wang et al [31] inferred VIV induced maximum fatigue damage at touchdown point is affected by trench depth, vertical and lateral stiffness and clay suction from their studies of VIV fatigue damage of SCR zone using time domain approach. Further studies in factors contributing to fatigue damage concentration at touchdown point of riser have to be performed for more accurate simulation of VIV-related fatigue damage.

CHAPTER 3

METHODOLOGY/ PROJECT WORK

This chapter describes the research procedure and management devised in order to achieve the objectives. The content discusses the outline of the research method to develop a novel simplified approach to assess fatigue performance of SCR. A clear description of identified key milestones and Gantt chart are included.

3.1 Research Methodology

In order to develop the simplified approach of assessing fatigue damage of SCR, the effect of current profile on the fatigue performance of SCR needs to be investigated. The flowchart in Figure 3.1 presents the research procedure to assess the VIV fatigue performance of SCR under the influence of various current profiles.

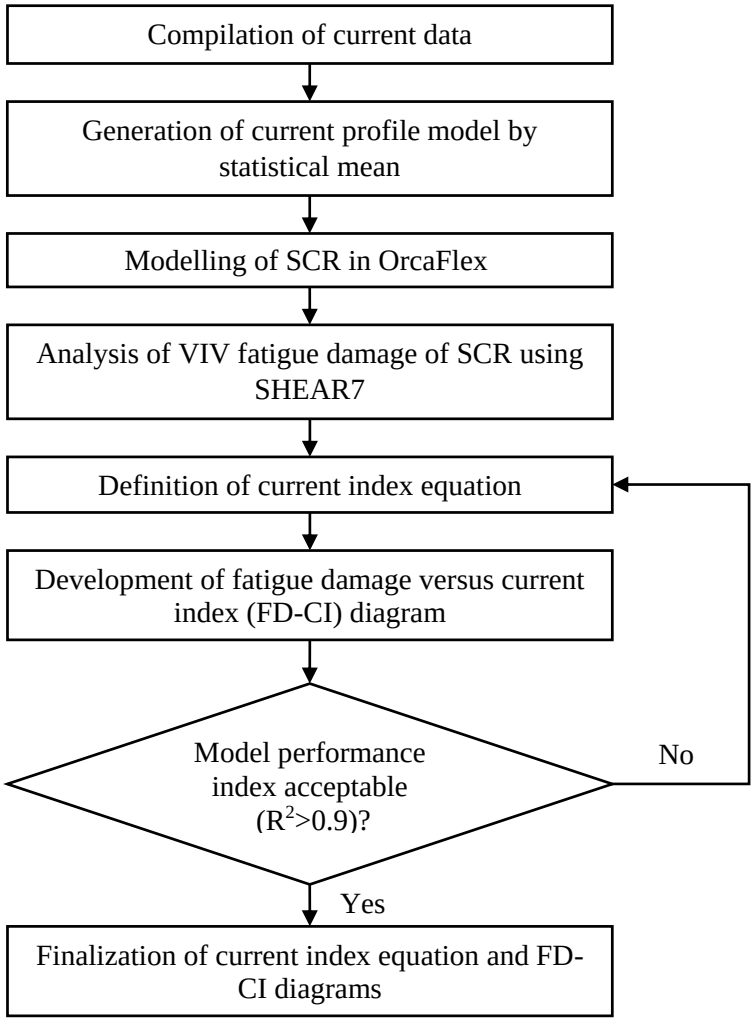

FIGURE 3.1: General procedure of analysis

3.1.1 Compilation of Current Data

At the beginning of analysis, current profile data from different regions around the world, especially oil and gas field development regions, were collected from design documents, reports and journal papers. These current profiles were compiled into a single graph.

3.1.2 Generation of Current Profile Model by Statistical Mean

The parameters that characterise the current profiles such as current speed and depth were distinguished. These parameters are used to produce probability density distribution of the current profiles. A three dimensional current profile model was developed from the collected current data based on the probability density distribution of the actual current profiles.

3.1.3 Modelling of SCR in OrcaFlex

SCR model was drawn in OrcaFlex using the structural data and environmental data with reference to thesis paper by Park [32]. Only SCR was modelled because SCR is the main concern in the VIV fatigue analysis. After drawing the SCR model, static configuration analysis of the SCR without environmental loading was performed to find the equilibrium configuration of the riser upon the exertion of static loading such as weight and buoyancy of the riser. With the input of the top end location of SCR, length of SCR, water depth and internal content of SCR, the bottom end of riser on seabed was located using the given hang-off angle. The touchdown point of the riser under static loading was determined through static analysis [33]. Strakes, which is commonly used to reduce VIV, were installed onto the riser model with 80 percent of coverage along the length of riser from the top end to touchdown point of riser to stimulate the real-life condition of riser in industry.

3.1.4 Analysis of VIV Fatigue Damage of SCR for Selected Current Profile Scenarios

To perform the sensitivity study of the VIV fatigue of SCR due to current, a total of 60 current profiles scenarios were generated from simplified current profile and applied to the same SCR model respectively to compute the fatigue damage along the length of SCR. The other environmental inputs such as wave and wind data remained

constant for all scenarios. By this means, the effects of current profile on fatigue damage of SCR can be determined. Using OrcaFlex coupled with SHEAR7, VIV fatigue damage of SCR was calculated for each current profile scenarios.

For each current profile scenarios, fatigue damage was analysed in 2 current heading direction, mainly 0 degree and 180 degree direction with respect to riser plane. After the fatigue damage was calculated for each current scenarios in both current directions for all SCR models, the results were compiled and tabulated. Maximum fatigue damage in each scenario was determined.

3.1.5 Definition of Current Index Equation

Current index formula was developed based on different principles. It was expressed as function of current velocity and water depth. The current index for each scenario was calculated using the developed method.

3.1.6 Development of Fatigue Damage versus Current Index (FD-CI) Diagrams

Using current index and fatigue damage calculated in previous steps for each current profile scenario, point scatter diagram of fatigue damage versus current index was plotted. Point representing maximum fatigue damage for each current scenario was plotted for each case of current heading direction in FD-CI diagram. A best fit regression line was drawn along these points. Equation for the regression line was computed and model performance index, R-squared statistic (R^2), was used to analyse how well fit are the points with the regression line.

3.1.7 Finalization of Current Index Equation and FD-CI Diagrams

Formulation of current index and plotting of FD-CI diagrams were repeated if R^2 was less than 0.9, in order to find the equation that can best describe the relation between current profile and fatigue damage. The current index formula that produced FD-CI diagrams with the highest R^2 value and best fit plot was chosen as the final equation of current index. These established FD-CI diagrams are expected to be able to ease the interpretation of fatigue damage suffered by SCR due to different current loads during design analysis process of SCR. The application of current index and FD-CI diagram is validated by comparing the estimated fatigue damage with computation result using SHEAR7. More detailed project activities are explained in the next two chapters.

CHAPTER 4

GENERATION OF CURRENT PROFILE MODEL

This chapter shows the project activities and results of the current profile model generation by statistical means for the subsequent investigation of relationship between current profile and fatigue damage of SCR. The complete process of producing the current profile model from the real current profile data using statistical approach is described and the results from the statistical analysis of the current profile and current profile model are presented in the following section.

4.1 Compilation of Current Data

The generation of current profile model was started with collection of current data from various deepwater regions with water depth greater than 500 m. A total of 54 current data was collected from regions such as Gulf of Mexico, North Sea, Brazil, West Africa, Borneo and Atlantic Frontier. The return period of the current ranges from 1 year to 1000 year. The current profile was summarized in Figure 4.1(a) below. The current velocity from the actual data is then plotted along normalized water depth as shown in Figure 4.1(b). With the use of normalized water depth current profile data, a current profile model was created using statistical mean.

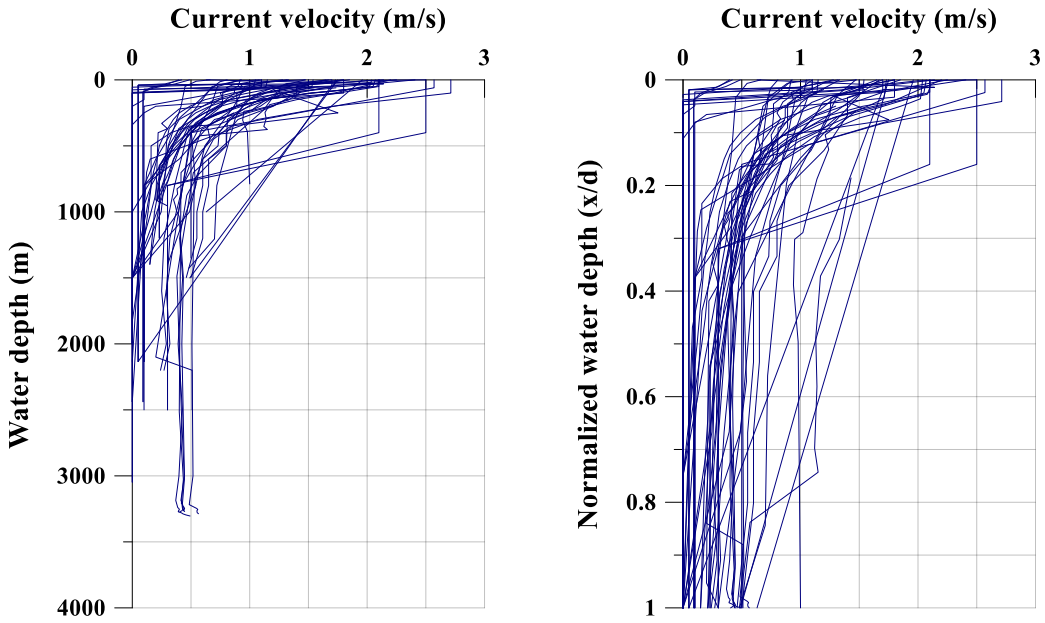

(a) Actual current profile (b) Normalized water depth current profile

FIGURE 4.1: Compilation of current profile

4.2 Generation of Current Profile Model by Statistical Mean

In the first step of analysis of the current profile data, the current velocities were determined at each normalised water depth (x/d) starting at x/d of 0, with an increment of 0.05, until x/d of 1. The current velocities were statistically analysed at each normalized water depth to determine the probability distribution of the velocity at each normalized water depth using goodness-of-fit test. The best probability distribution function of the current velocities along the normalized water depth was determined by using Anderson-Darling test. The Anderson-Darling statistic is expressed as below:

$$A^2 = -n - \left(\frac{1}{n}\right)\sum_i \left[\left(2i-1\right)\log Z_{(i)} + \left(2n+1-2i\right)\log\left(1-Z_{(i)}\right)\right] \tag{4.1}$$

where Z is used to represent F(X) which is the cumulative distribution function of the data [34]. Given a sample X_1 until X_n, $Z_{(i)}$ is represented as

$$Z_{(i)} = F(X_i),\ i = 1,...,n, \tag{4.2}$$

The Anderson-Darling statistic shows how well fitted is the distribution for data from the fitted line in probability plot. Hence, by applying several probability distribution, the Anderson-Darling statistic was determined using the software, Minitab. The smaller the statistic, the better the distribution fits the data. Since current velocities data had different best-fitted distribution at each normalized water depth, the lowest average of the total Anderson-Darling statistics is determined to identify a single distribution that can represent the overall progress of current velocity along the normalized water depth. The current velocity at each normalized water depth is represented in the form of probability density function and histogram.

The bin width of the histogram has a significant effect on the statistical properties of the data, hence the best bin width, h, for each normalized water depth was identified using Scott's normal reference rule which is calculated using the equation below

$$h = \frac{3.5\hat{\sigma}}{n^{1/3}} \tag{4.3}$$

where $\hat{\sigma}$ is the sample standard deviation and n is total number of data points used in the sample [35]. The results of the goodness-of-fit and bin width calculation were shown in probability density functions and histograms in the next chapter. From the statistical analysis, the current profile model was developed.

4.3 Results

4.3.1 Statistical Analysis Result of Real Current Profile

The best probability distribution and histogram to represent the current velocity distribution at each normalized water depth are identified and presented in Figure C.1 to C.7 in Appendix C. In each graph, three probability density distributions are presented. Original distribution is the best fit distribution at each normalized water depth, which means different distribution is identified for current velocity at each normalized water depth (x/d). For instance, the best fit distribution at x/d=0 is normal distribution whereas the best fit distribution at x/d=0.05 is logistic distribution. Optimized distribution represents the overall best fit distribution considering all normalized water depths, which is determined from the lowest overall average Anderson-Darling statistics.

The overall best fit probability density distribution that can represent the progress of current velocity along the normalized water depth is extreme value distribution. The extreme value distribution function used to plot the graph, as shown in Figure 4.2, is represented in the Equation 4.4 below in terms of location parameter (μ) and scale parameter (σ) with current velocity as the variable x.

$$f(x) = \left(\frac{1}{\sigma}\right) \cdot \exp\left[-\frac{(x-\mu)}{\sigma}\right] \cdot \exp\left\{-\exp\left[-\frac{(x-\mu)}{\sigma}\right]\right\} \tag{4.4}$$

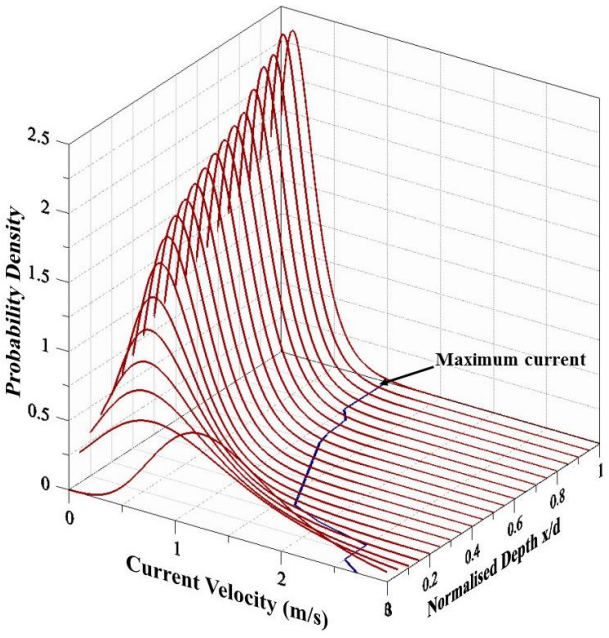

FIGURE 4.2: Probability density of actual current velocity along normalised depth

The location and scale parameter are formulated as the function of normalized water depth. As shown in Figure 4.3 and 4.4, these parameters vary with the normalized water depth in a consistent trend that can be represented as equation. Rational function is found to be the best fit to describe the relationship between location parameter and normalized water depth whereas third order polynomial can well relate the normalized water depth to the scale parameter. This is proven by the high coefficient of determination, R-squared value (R^2). The closer the R^2 to 1, the better fit is the function. Hence, the location parameter (μ) and scale parameter (σ) can be estimated using the function of normalized water depth (x/d) as shown below.

$$\mu = \frac{0.05222\left(x/d\right)+0.08350}{\left(x/d\right)+0.0670} \tag{4.5}$$

$$\sigma = -1.163\left(x/d\right)^3 + 2.429\left(x/d\right)^2 - 1.743\left(x/d\right)+0.6154 \tag{4.6}$$

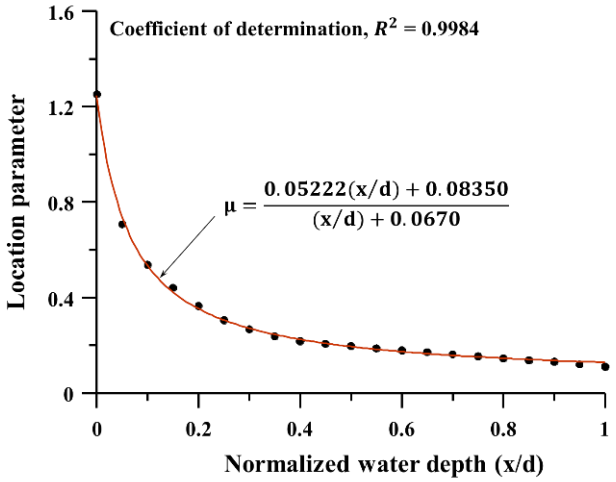

FIGURE 4.3: Relationship of location parameter with normalized water depth

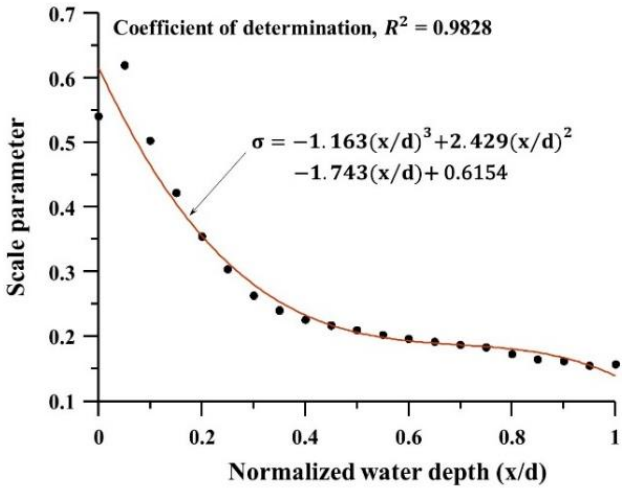

FIGURE 4.4: Relationship of scale parameter with normalized water depth

4.3.1 Current Profile Model

By inserting the location and scale parameter into the extreme distribution function, the current profile model can be developed. The current profile model is approximated and developed using the equations as follow.

$$f_v = \left(\frac{1}{\sigma}\right) \cdot \exp\left[-\frac{(v-\mu)}{\sigma}\right] \cdot \exp\left\{-\exp\left[-\frac{(v-\mu)}{\sigma}\right]\right\} \tag{4.7}$$

where f_v is the probability density of current velocity, v is the current velocity and

$$\mu = \frac{0.05222(x/d) + 0.08350}{(x/d) + 0.0670}$$

$$\sigma = -1.16(x/d)^3 + 2.43(x/d)^2 - 1.74(x/d) + 0.615$$

These equations are used to formulate the distribution function which is represented as approximate distribution function shown in Figure C.1 to C.7 in Appendix C. These approximate distribution functions are used to determine the probability of occurrence of a certain current velocity at the specified normalized water depth. The current profile model is then developed by combining all the approximate probability distribution function, as illustrated in Figure 4.5. This current profile model can be applied in determining the most representative current profile for fatigue assessment based on mean and standard deviation of the statistical model.

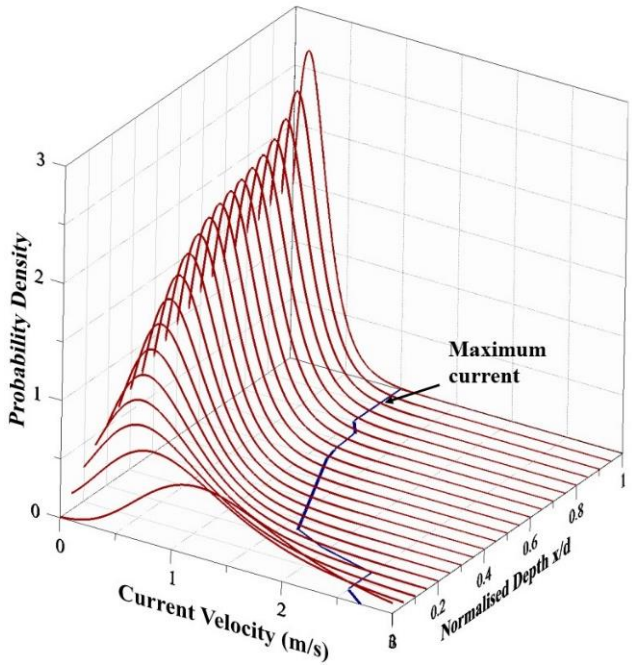

FIGURE 4.5: Current profile model along normalized water depth using approximate probability density distribution

CHAPTER 5

DEVELOPMENT OF CURRENT INDEX AND FD-CI DIAGRAM

This chapter shows the project activities, results and discussions of the current index and fatigue damage-current index (FD-CI) diagrams development by analysing fatigue damage of SCR. Comprehensive explanation of the steps taken, including modelling of SCR, analysis of VIV fatigue damage of SCR, definition of current index equation and development of FD-CI diagrams are covered in this chapter. The result from the VIV fatigue analysis from the perspective of the model analysis and fatigue damage analysis, final current index equation and FD-CI diagrams are presented. Validation study and consequent results are discussed in the following section.

5.1 Modelling of SCR

SCR model was drawn in OrcaFlex using the structural data and environmental data with reference to thesis paper by Park [32] as shown in Figure 5.1. Several design codes were used in designing feasible SCR for this study such as:

- API RP 2RD, "Design of risers for floating production systems (FPSs) and tension leg platforms (TLPs)", 2006 [36].
- DNV RP F204, "Riser fatigue", 2010 [37].

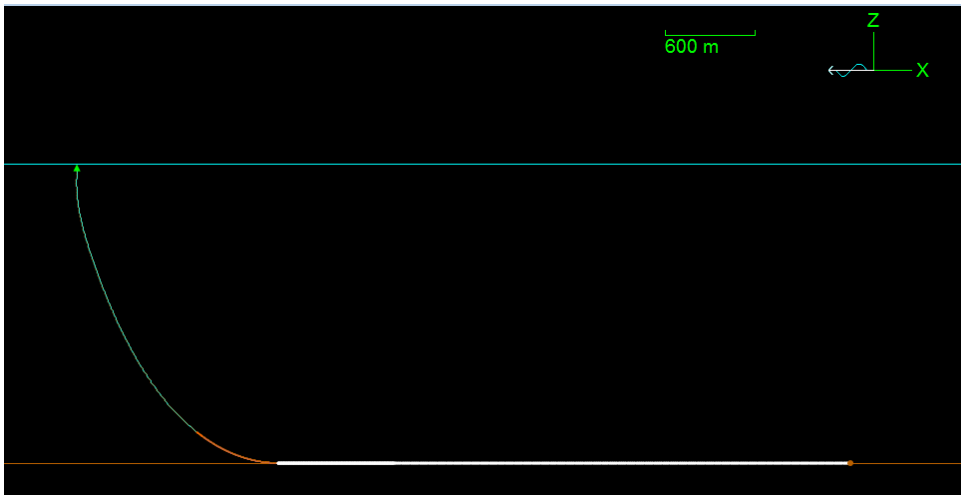

FIGURE 5.1: SCR model in OrcaFlex

In the model, the coordinate system was defined as such: x-axis is horizontal axis along the riser plane parallel to the portion of riser laying on the seabed; y-axis is perpendicular to the riser plane; z-axis is the vertical axis along the riser plane

representing the water depth. The selected water depth was 2000m. The host platform of the model was semi-submersible. A 10 inch SCR was modelled with tapered stress joint (TSJ) installed within the porch at the point of hang-off of the riser to increase the stiffness of the riser and prevent over-bending at the hang-off zone of the SCR. Only SCR was modelled and the top end of the SCR was set to be fixed, assuming vessel motion is fixed, in order to investigate VIV fatigue damage of SCR caused purely by current. The details of the SCR model and input data used for modelling are presented in Appendix A.

After drawing the SCR model, static configuration analysis of the SCR without environmental loading was performed to compute the catenary equation and find the equilibrium configuration of the riser. Static analysis was then conducted with exertion of environmental loading to determine the touchdown point of the riser. Modelling of strakes on the riser was performed by using 80 percent of coverage of strakes along the length of riser from the top end to touchdown point of riser as shown in Figure 5.2. Static configuration analysis and static analysis were performed again to determine the final touchdown point of SCR with the attachment of strakes.

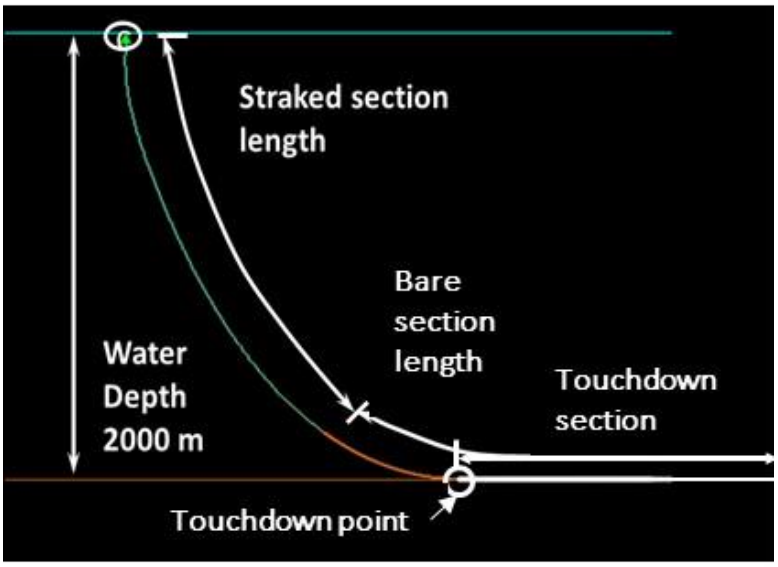

FIGURE 5.2: SCR model with section definition

5.2 Analysis of VIV Fatigue Damage of SCR for Selected Current Profile Scenarios

5.2.1 Selection of Current Profile Scenarios

Simplified current profiles that represent the critical current profiles at each offshore development regions, as shown in Figure 5.3, were determined from the real current profiles. Based on the representative current profile from each offshore development regions [3], the maximum and minimum current profile were identified and defined as shown in Figure 5.3. To understand the relationship between current profile and fatigue damage of SCR, a total of 60 current profile scenarios was generated within the boundary of maximum and minimum current profiles by varying parameters defined in Figure 5.4, such as surface and bottom current velocity and the profile gradient. The current profile was divided into 3 regions based on the profile gradient of the current. The parameter y_1, y_2, and y_3 define the depth of each region and x_1, x_2, x_3, and x_4 are the current velocity at each depth.

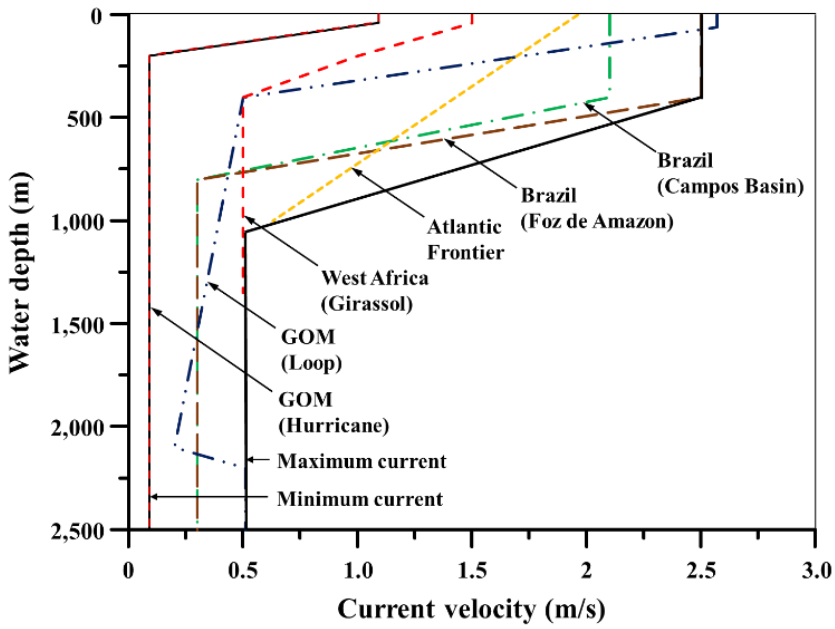

FIGURE 5.3: Representative current profile for different regions

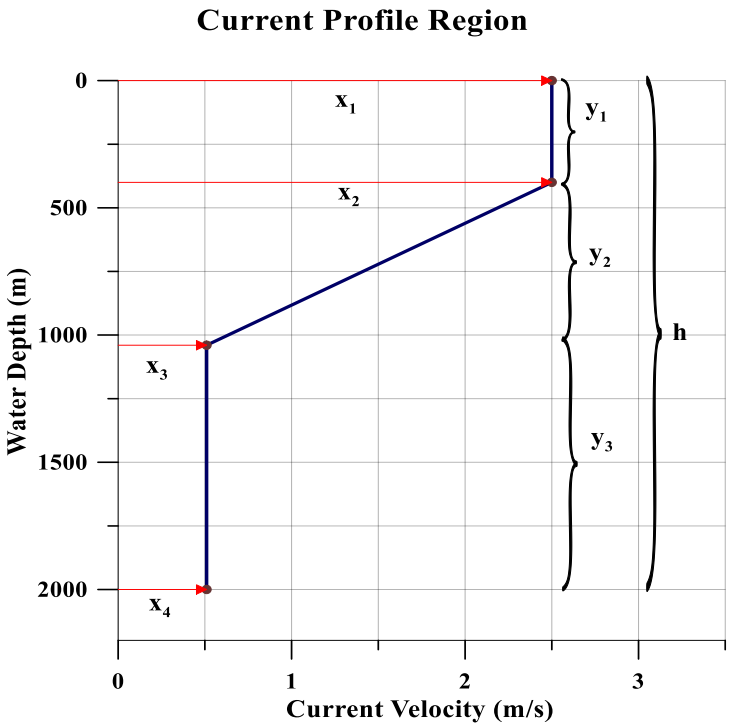

FIGURE 5.4: Definition of current profile shape and parameter

Figure 5.5 shows the 60 current profile scenarios to be analysed. Static strength analysis were performed using the SCR model drawn in OrcaFlex, stated in previous section, for each current profile scenario to ensure the SCR model will not fail under static loading. According to design code such as API RP 2RD [36], utilization of a practical riser design must be less than or equal to 1. Utilization with value greater than 1 indicates stress exceeds the yield strength of the riser, which will lead to failure. Scenario with utilization more than 1 implies the design of SCR is unacceptable for the certain current loads and it has to be discarded. Among the 60 scenarios, 14 current profile scenarios were discarded and Table 5.1 shows the remaining 46 scenarios which were used to perform subsequent VIV fatigue analysis.

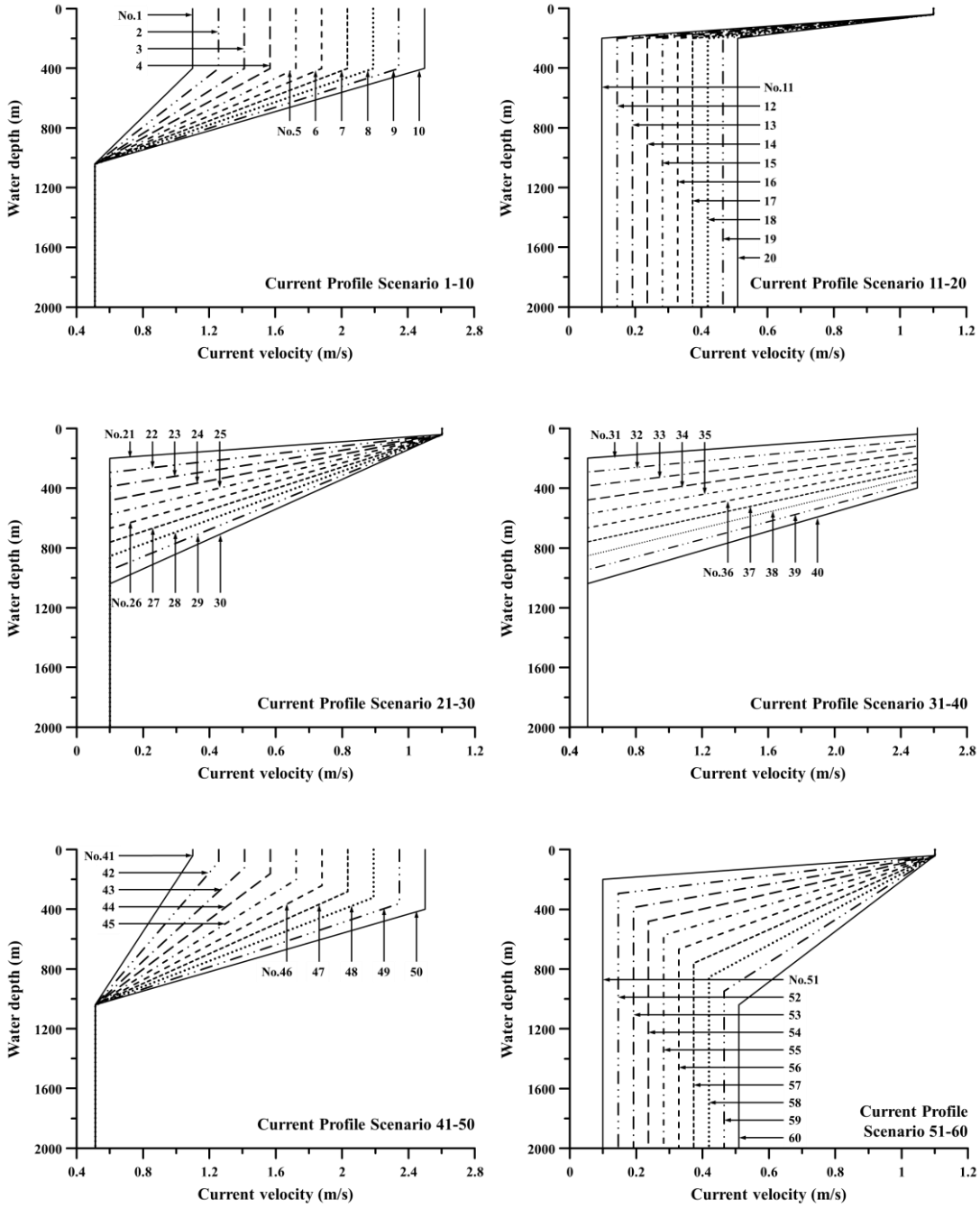

FIGURE 5.5: Individual current profile scenarios

TABLE 5.1: Current parameters for all 46 current profile scenarios

No.	Scenarios	Velocity (m/s)		Region depth (m)		
		Surface (V_0, V_1)	Bottom (V_2, V_3)	y_1	y_2	y_3
1	1	1.100	0.510	400	640	960
2	2	1.256	0.510	400	640	960
3	3	1.411	0.510	400	640	960
4	4	1.567	0.510	400	640	960
5	5	1.722	0.510	400	640	960
6	6	1.878	0.510	400	640	960
7	11	1.100	0.100	40	160	1800
8	12	1.100	0.146	40	160	1800
9	13	1.100	0.191	40	160	1800
10	14	1.100	0.237	40	160	1800
11	15	1.100	0.282	40	160	1800
12	16	1.100	0.328	40	160	1800
13	17	1.100	0.373	40	160	1800
14	18	1.100	0.419	40	160	1800
15	19	1.100	0.464	40	160	1800
16	20	1.100	0.510	40	160	1800
17	22	1.100	0.100	40	253	1707
18	23	1.100	0.100	40	347	1613
19	24	1.100	0.100	40	440	1520
20	25	1.100	0.100	40	533	1427
21	26	1.100	0.100	40	627	1333
22	27	1.100	0.100	40	720	1240
23	28	1.100	0.100	40	813	1147
24	29	1.100	0.100	40	907	1053
25	30	1.100	0.100	40	1000	960
26	31	2.500	0.510	40	160	1800
27	32	2.500	0.510	80	213	1707
28	33	2.500	0.510	120	267	1613
29	34	2.500	0.510	160	320	1520
30	35	2.500	0.510	200	373	1427
31	36	2.500	0.510	240	427	1333
32	41	1.100	0.510	40	1000	960
33	42	1.256	0.510	80	960	960
34	43	1.411	0.510	120	920	960
35	44	1.567	0.510	160	880	960
36	45	1.722	0.510	200	840	960
37	46	1.878	0.510	240	800	960
38	47	2.500	0.510	400	640	960
39	52	1.100	0.146	40	253	1707
40	53	1.100	0.191	40	347	1613
41	54	1.100	0.237	40	440	1520
42	55	1.100	0.282	40	533	1427
43	56	1.100	0.328	40	627	1333
44	57	1.100	0.373	40	720	1240
45	58	1.100	0.419	40	813	1147
46	59	1.100	0.464	40	907	1053

5.2.1 VIV Fatigue Analysis

VIV fatigue analysis were performed on the SCR model for uniform current profile at first as the base case to investigate the influence of current velocity to fatigue damage. The current velocities used for the analysis were 0.1, 0.28, 0.46, 0.65, 0.83, 1.01, 1.19 and 1.28 m/s. After that, VIV fatigue analysis were conducted for all the 46 sheared current profile scenarios with water depth of 2000m. OrcaFlex coupled with SHEAR7 software was utilised to calculate VIV fatigue damage of SCR. VIV response of the riser structure was calculated using equation of motion which is defined as follow.

$$m_t \ddot{y} + R\dot{y} - Ty'' = P(x,t) \tag{5.1}$$

where m_t is the mass per unit length including the added mass, R is the damping per unit length including strutural and hydrodynamic damping, T is the tension, $\ddot{y}$ is the acceleration of the structure, $\dot{y}$ is the velocity of the structure, y" is the second derivative of the displacement of the structure with respect to spatial variable, x and t are spatial and temporal variable and $P(x,t)$ is the lift force per unit length with frequency ω of the structure as follows.

$$P(x,t) = \frac{1}{2}\rho_t D V^2(x) C_L(x;\omega_r)\sin(\omega_r t) \tag{5.2}$$

where ρ_f is the fluid volume density, D is the diameter of the cylinder, $V(x)$ is the velocity of flow and $C_L(\mathrm{x};\omega_r)$ is the lift coefficient of mode r and r is the mode number. The RMS stress was computed using mode superposition approach and short-term VIV fatigue damage rate was determined using S-N curve and Miner rule in SHEAR7 [19], [32].

Stress concentration factor for SCR was assumed to be 1.1 for all welded connections along SCR except TSJ. DNV C (DNV RP C203) single slope S-N curve with cathodic protection for X65/X65 welds was used in fatigue life calculation of SCR and RITES was used for calculation at TSJ. Equation of the S-N curve is defined as below:

$$\Delta\sigma = \left(\frac{10^a}{N}\right)^{1/b} \tag{5.3}$$

where $\Delta\sigma$ is hot spot nominal stress range, N is the number of cycle to failure, a is the intercept on cycle axis for S-N curve and b is slope of S-N curve, which is presented in Table A7 in Appendix A.

Fatigue damage of the SCR was analysed in 2 current heading directions: 0 and 180 degree with respect to the positive x-axis of the riser plane as shown in Figure 5.6. Current heading direction of 0 degree represents near case in which vessel and top end of the riser move towards touchdown point of riser, whereas 180 degree direction represents far case in which vessel and top end of the riser drift away from touchdown point of riser.

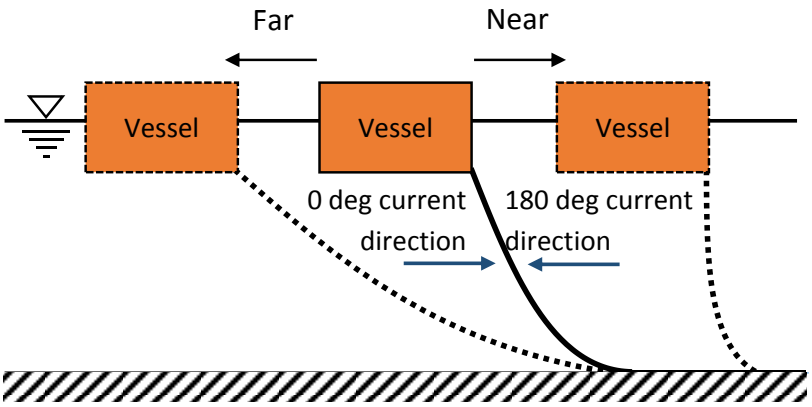

FIGURE 5.6: Motion of riser with respect to current heading direction

There are two types of fatigue damage calculations, which are short-term and long term fatigue damage. In this study, only short-term VIV fatigue damage is considered for investigation of current effect to VIV fatigue damage of riser. The allowable maximum fatigue damage is 1.0 over the period of the short-term event based on design code, DNV RP F204 [37]. The results of the VIV fatigue analysis are presented in the next chapter.

5.3 Results

5.3.1 Fatigue Analysis Result for Uniform Profile

The VIV fatigue damage of the SCR under influence of uniform current profile of different magnitude is investigated. The fatigue damage distribution along the riser length is studied, as plotted in Figure 5.7. The graph shows the fatigue damage concentrates around the section 2000m to 2600m which is touchdown zone of the riser. As the current velocity increases, the fatigue damage rate increases. The maximum fatigue damage of the riser increases with the increasing current velocity as plotted in Figure 5.8, due to the higher mode being excited in higher current velocity condition, leading to greater modal curvature and greater fatigue damage rate. The result is consistent with previous studies done by Gao et al. [27]. The relationship between the current velocity and maximum fatigue damage of the riser can be described using empirical equation derived from the best-fitted line, such that maximum fatigue damage is proportional to current velocity raised to the power of 4.4. The high R^2 value of the empirical equation suggests the equation is suitable to describe the correlation between current velocity and maximum fatigue damage.

$$FD = 0.003350 \cdot V^{4.4} \tag{5.4}$$

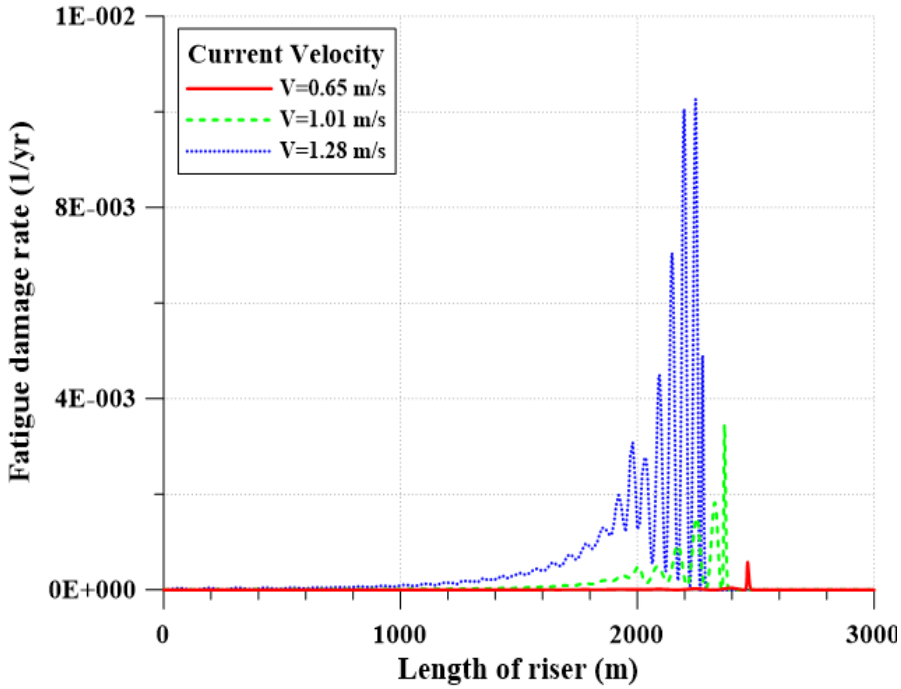

FIGURE 5.7: Fatigue damage rate along whole riser

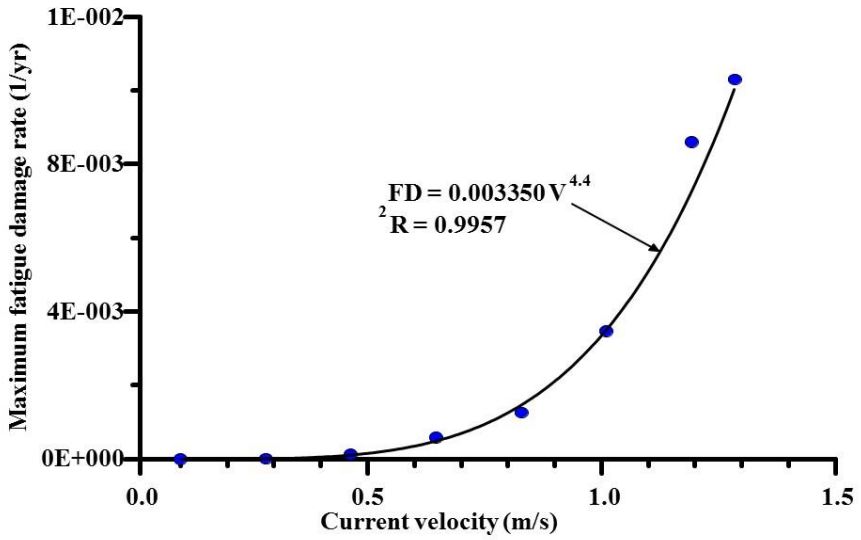

FIGURE 5.8: Maximum fatigue damage versus current velocity

5.3.2 VIV Analysis Result for Selected Sheared Current Profile Scenarios

5.3.2.1 Modal Analysis

Modal analysis is performed to identify the potentially excited modes that contribute to VIV. The modes are excited when the modal (natural) frequency of the riser structure is equal or near to the vortex shedding frequency. Using SHEAR7, the total modal power generated by each vibration mode is estimated and plotted in Figure 5.9 for each scenarios. As observed from Figure 5.9, most scenarios show two peaks of modal power except scenarios 11 to 20. The first peak occurs before mode number 12 and the second peak occurs after mode number 12.

The dominant mode is the mode with the highest modal power. For scenarios 1 to 6, 11 to 20 and 41 to 47, which current velocity is increasing, it is observed that the dominant mode is greater. This implies the higher the current velocity, the higher the dominant excited mode that contributes to VIV. For scenarios 22 to 30 and 31 to 36, which surface and bottom current velocity is constant, the dominant mode remain constant, with increasing modal power. Hence, it can be deduced that the current velocity governs the dominant excited mode since the higher the current velocity, the higher is vortex shedding frequency, therefore higher modes with greater modal frequency are excited.

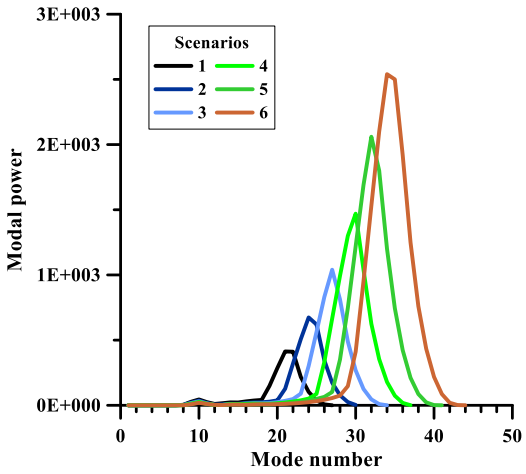

(a) Scenario 1 to 6

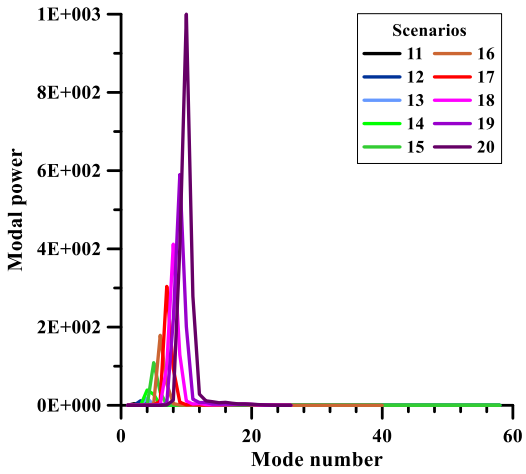

(b) Scenario 11 to 20

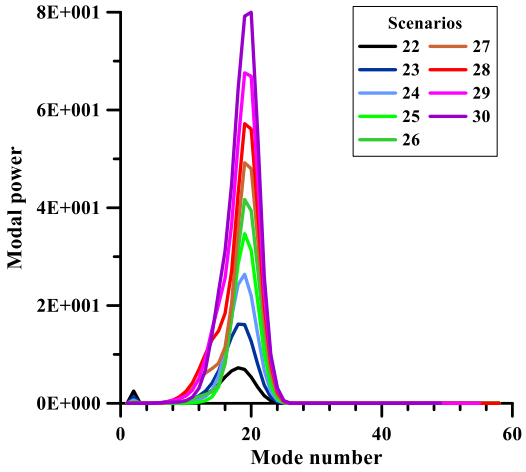

(c) Scenario 22 to 30

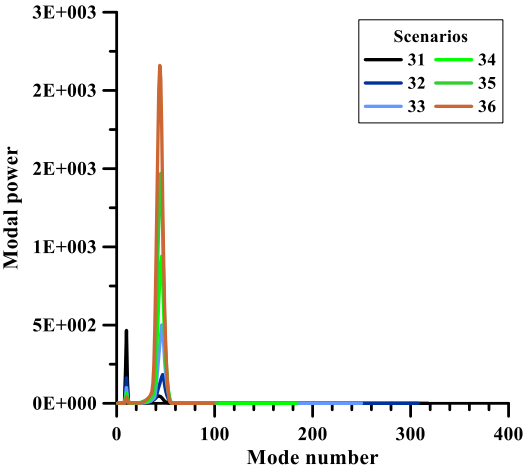

(d) Scenario 31 to 36

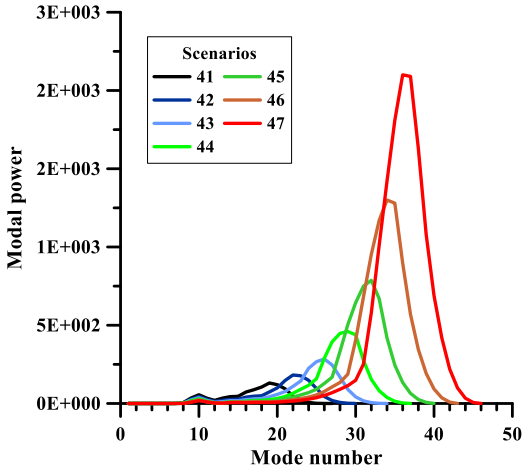

(e) Scenario 41 to 47

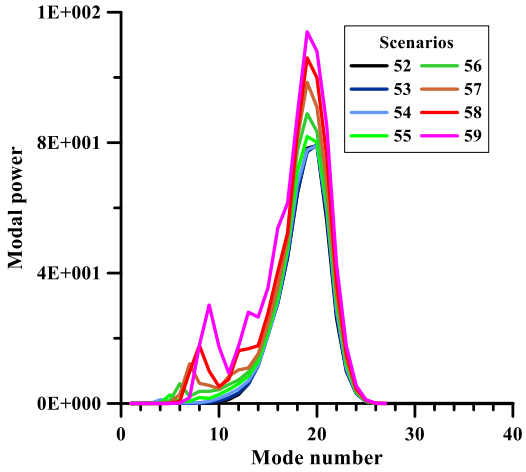

(f) Scenario 52 to 59

FIGURE 5.9: Modal power versus mode number for all scenarios.

5.3.2.2 VIV Fatigue Analysis Result

To develop the current index equation and establish the relationship between shear current profile and VIV fatigue damage, the VIV fatigue performance of the SCR model is analysed in 46 scenarios of different current profile loadings, as presented in Table 5.1, for 2 current heading direction, 0 (near case) and 180 degree (far case). All the 46 current profiles scenarios have same shape but are scaled differently by varying the current velocity at different point of water depth. The maximum fatigue damage rate of the SCR for each scenario for near case and far case is summarized in Figure 5.10(a) and Figure 5.10(b) respectively. Figure 5.11 shows the location along the riser for each case where maximum fatigue damage is identified in each scenario, with 0m as the top end of the riser. Section of the riser starting from 0m to 500m is defined as hang-off zone, where the riser is attached to vessel. Section of riser begins at 2100m to 2600m is defined as touchdown zone, where the riser touches the seabed.

As observed from Figure 5.10, the maximum fatigue damage for all scenarios are similar in both near and far case. From Figure 5.10, in both near and far case, for scenario 1 to 6 in which the surface current velocity is increasing, the maximum fatigue damage rate is found to be increasing with the increasing surface current velocity from scenario 1 to 6. Similarly, the maximum fatigue damage rate is observed to be increasing as the bottom current velocity increases from scenario 11 to 20. These results are in agreement with the results for uniform current profile in Section 5.3.1, since the higher dominant excited mode of the riser structure is excited when current velocity increases, causing higher frequency of vibration and greater curvature, leading to greater fatigue damage as shown in Figure 5.9(a) presented in previous sub-section. The maximum fatigue damages for scenario 1 to 6 are identified near the hang off point of the SCR due to high current velocity at surface, whereas maximum fatigue damages in scenario 11 to 20 occur near touchdown point of the riser due to high current velocity near the seabed, as portrayed in Figure 5.11.

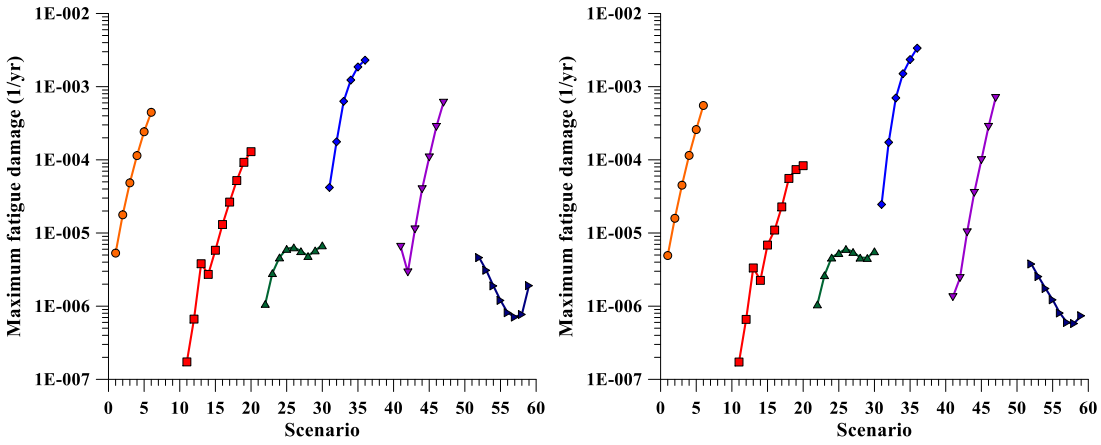

(a) 0 degree current heading direction (Near case)

(b) 180 degree current heading direction (Far case)

FIGURE 5.10: Maximum fatigue damage for all 46 current profile scenarios

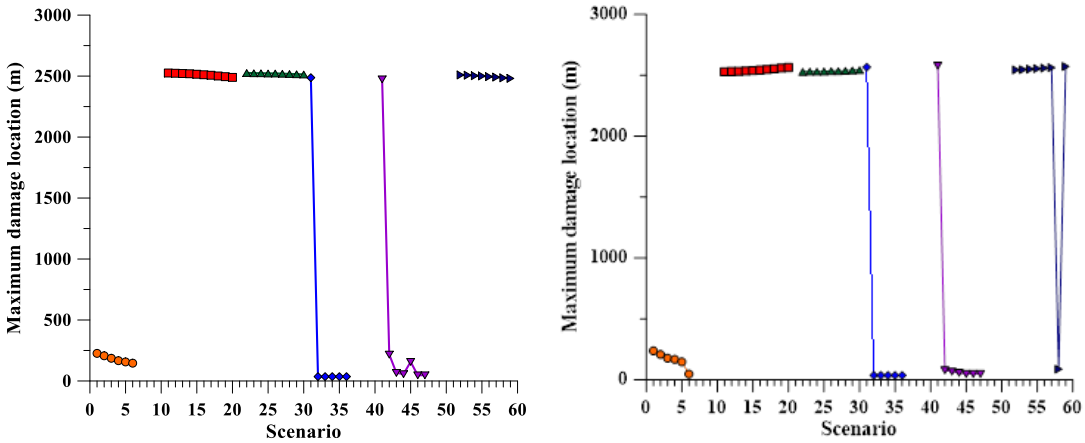

(a) 0 degree current heading direction (Near case)

(b) 180 degree current heading direction (Far case)

FIGURE 5.11: Maximum fatigue damage location for all 46 current profile scenarios

In scenario 22 to 30 and scenario 31 to 36, the surface current and bottom current velocity are constant while the shear gradient in mid-section of the current profile changes. In both near and far cases, the maximum fatigue damage generally increases with the shear gradient due to the increase of current velocity at the mid-section of the current profile from scenario 22 to 30 and scenario 31 to 36. However, in scenario 25 to 29, the maximum fatigue damage fluctuates. This is caused by the distribution of fatigue damage along the arc length of the riser which can be observed in Figure 5.12(a) and 5.12(b). The zoom-in plot in Figure 5.12(b) shows that fatigue damages along the riser length at the touchdown zone. The maximum fatigue damage are less for scenario 27 to 29 than scenario 25 and 26. This is because the fatigue damages are more

distributed for scenario 27 to 29 than scenario 25 and 26 since more modes are excited in scenario 27 to 29 as shown in Figure 5.9(c) in previous section, resulting in less critical fatigue damage. In scenario 22 to 30, all the fatigue damages occur at touchdown zone whereas in scenario 31 to 36, all maximum fatigue damages happen at hang-off zone except scenario 31.

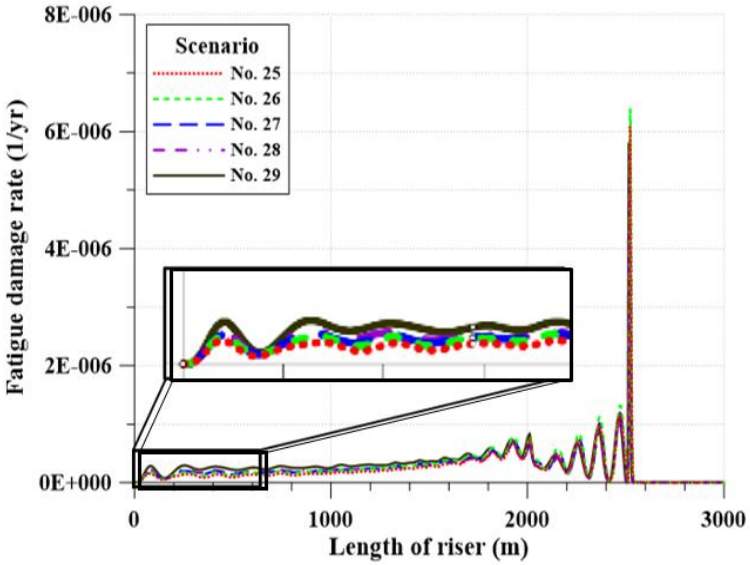

(a) Fatigue damage rate along whole riser

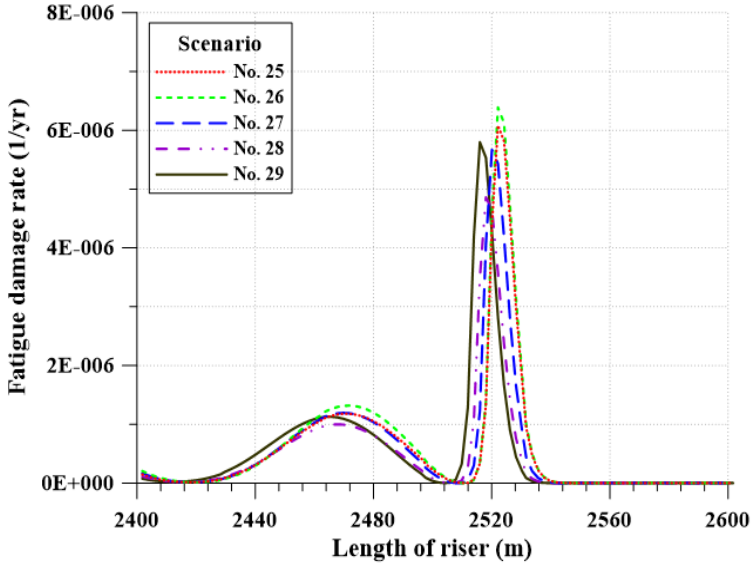

(b) Fatigue damage rate at touchdown zone

FIGURE 5.12: VIV fatigue damage result for scenario 25 to 29

In scenario 41 to 47 and scenario 52 to 59, the current velocity varies along the water depth. In far case, the maximum fatigue damage rate increases from scenario 41 till 47 since the surface current velocity increases, resulting in excitation of high mode number with greater modal frequency. However, in near case, the maximum fatigue damage rate decreases from scenario 41 to 42 and increases consequently. The drop and rise of the maximum fatigue damage rate can be explained by the change in the maximum fatigue damage location, as shown in Figure 5.11(b) and Figure 5.13. In Figure 5.13, two peaks can be noticed along the riser length. The first peak occurs around hang-off zone and the second peak occurs near the touchdown zone. Scenario 41 has maximum fatigue damage at the second peak while scenario 42 and 43 have maximum fatigue damage at the first peak.

Likewise, in both near and far case for scenario 52 to 59, two peaks are observed from the plot of fatigue damage distribution along riser length in Figure 5.14. The maximum fatigue damages in all the 8 scenarios occur at touchdown zone, but fatigue damages are well-distributed in scenario 56 and 57 and the bottom current velocity in scenario 58 and 59 are higher, which explain the drop and increase of the maximum fatigue damage.

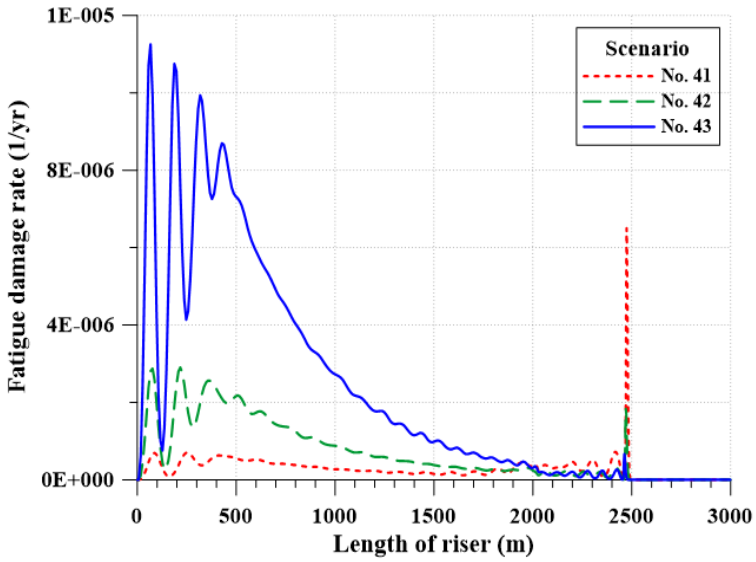

FIGURE 5.13: Fatigue damage rate along whole riser for scenario 41 to 43

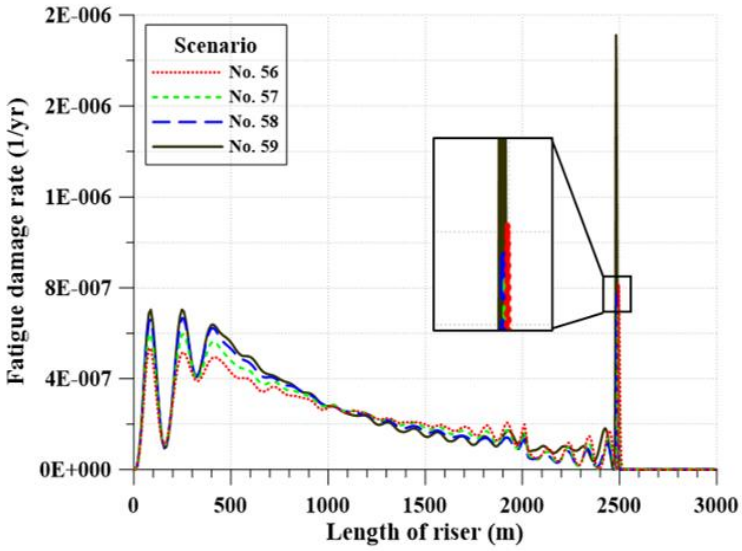

FIGURE 5.14: Fatigue damage rate along whole riser for scenario 56 to 59

5.4 Discussions

From the VIV fatigue analysis result presented in previous sections, it can be observed that in uniform current profile cases, fatigue damage concentrates in touchdown zone in uniform profile case because of less mode being excited, while in sheared current profile cases, fatigue damage is more distributed along the riser length due to multiple mode excitation. In some cases which both top and bottom current velocity are high, two peaks of fatigue damage can be identified along the riser length. Regarding the relationship of the current profile with the fatigue damage, it can be deduced that maximum fatigue damage increases with increasing current velocity, which can be observed clearly in uniform current profile cases. The maximum fatigue damage is proportional to current velocity raised to the power of 4. The result is coherent with Gao et al. [27]. However, in sheared current profile cases, more modes are excited and the superposition of the mode shapes causes the distribution of fatigue damage along the riser and less concentration of fatigue damage in one section of riser, hence may reduce the overall maximum fatigue damage eventually even when current velocity is high.

Current index equation is developed and presented in the following section. The characteristics of current data (velocity and profile) are used to define current index which is a unique representative value for each current data.

5.4.1 Current Index Formulation

The current index equation is the function of the current velocity and water depth. The current profile is first divided into three regions according to the current velocity along the water depth. Definition of the parameters used in the current index equation can be referred to Figure 5.4. The current velocity is denoted as x and the subscript represents the region. Using the maximum fatigue damage equation, Equation 5.4, established in previous section, the current index equation is defined as below

$$CI = \sum_{i=1}^{n} \alpha_i \cdot V_i^4 \tag{5.5}$$

where n is the number of division of current profile, i is the region number, α is the region coefficient and V^4 is the integral of velocity along the water depth. The power of 4 is derived from Equation 5.4, which the power of 4.4 is rounded off to 4. The equation of V^4 is defined as below.

$$V_i^4 = \int \left[V(y) \right]^4 dy$$

$$V_i^4 = \int_0^{y_i} \left(\frac{x_{i+1} - x_i}{y_i - 0} \right) \bullet \left(y + \frac{y_i - 0}{x_{i+1} - x_i} x_i \right)^4 dy$$

$$V_i^4 = \frac{y_i}{5} \left(x_i^4 + x_i^3 x_{i+1} + x_i^2 x_{i+1}^2 + x_i x_i^3 + x_{i+1}^4 \right) \tag{5.6}$$

Hence, the complete current index equation is

$$CI = \sum_{i=1}^{n} \alpha_i \cdot \frac{y_i}{5} \left(x_i^4 + x_i^3 x_{i+1} + x_i^2 x_{i+1}^2 + x_i x_i^3 + x_{i+1}^4 \right) \tag{5.7}$$

Since the division of current profile region is based on the current profile and velocity variation, the region coefficient α is defined as the average velocity at that region. In the case of uniform profile, α is the constant velocity of the current region. In the case of shear profile, α is defined as the average of the velocity of the region.

For uniform profile: $$\alpha_i = V_i \quad (5.8a)$$

For shear profile: $$\alpha_i = \frac{V_i + V_{i+1}}{2} \quad (5.8b)$$

By applying the current index equation developed, current indices for all the 46 current profile scenarios are calculated and presented in Table 5.2.

TABLE 5.2: Current index value (CI) for all 46 current profile scenarios

No.	Scenarios	CI	No.	Scenarios	CI
1	1	9.526	**24**	29	2.397
2	2	17.489	**25**	30	2.577
3	3	30.299	**26**	31	63.309
4	4	49.911	**27**	32	110.214
5	5	78.751	**28**	33	157.120
6	6	119.763	**29**	34	204.025
7	11	0.954	**30**	35	250.931
8	12	0.982	**31**	36	297.836
9	13	1.015	**32**	41	5.276
10	14	1.056	**33**	42	9.842
11	15	1.111	**34**	43	17.952
12	16	1.188	**35**	44	31.695
13	17	1.295	**36**	45	54.016
14	18	1.446	**37**	46	88.920
15	19	1.659	**38**	47	141.710
16	20	1.953	**39**	52	1.178
17	22	1.134	**40**	53	1.441
18	23	1.314	**41**	54	1.752
19	24	1.495	**42**	55	2.120
20	25	1.675	**43**	56	2.556
21	26	1.855	**44**	57	3.075
22	27	2.036	**45**	58	3.690
23	28	2.216	**46**	59	4.418

5.4.2 Fatigue Damage-Current Index (FD-CI) Diagrams

The maximum fatigue damage versus current index (CI) for 0 degree (near case) and 180 degree (far case) current direction are plotted as shown in Figure 5.15 and Figure 5.16. These graphs are defined as Fatigue Damage-Current Index (FD-CI) Diagram. Empirical equation can be derived from the fitted line plotted through the data point. The high R^2 value indicates the empirical equation can be used to correlate the current

index and maximum fatigue damage and can be applied to estimate the maximum fatigue damage.

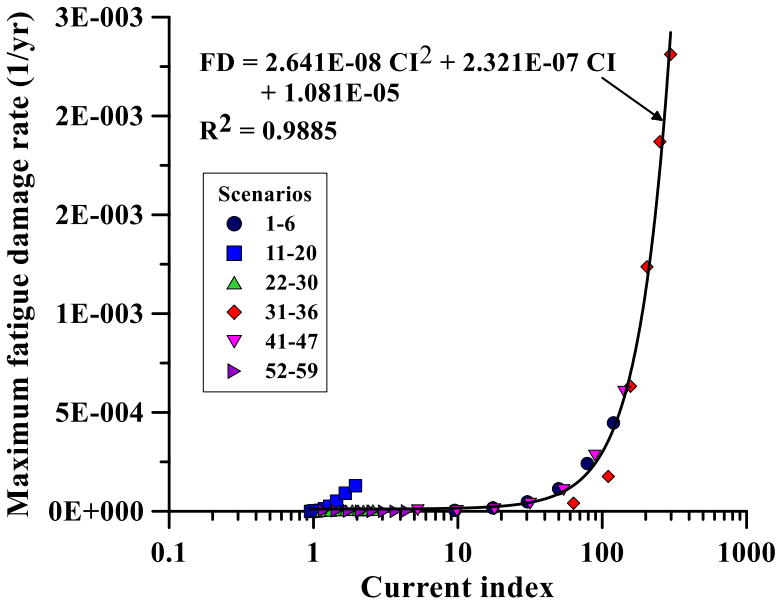

FIGURE 5.15: Fatigue Damage - Current Index (FD-CI) diagram at 0 degree current heading direction (Near case)

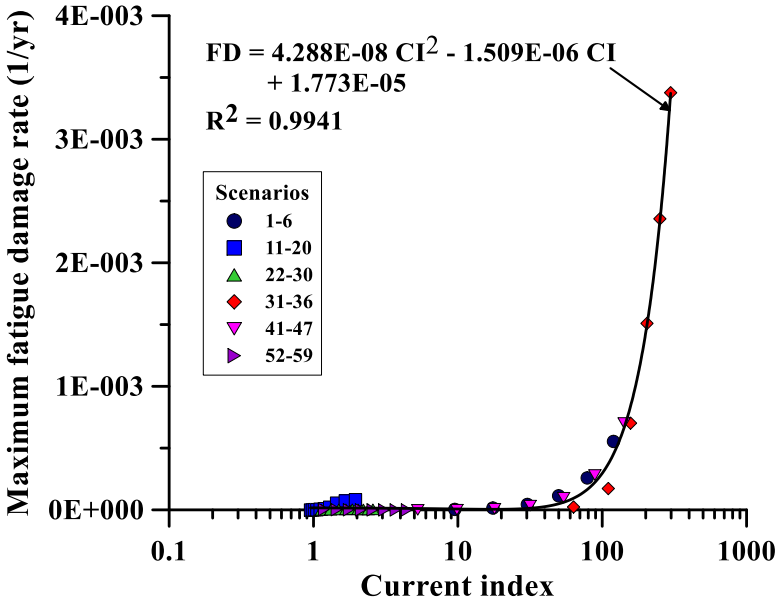

FIGURE 5.16: Fatigue Damage - Current Index (FD-CI) diagram at 180 degree current heading direction (Far case)

Figure 5.17 below shows the comparison of maximum fatigue damage for both 0 and 180 degree current heading direction. The maximum fatigue damage for both current

heading direction is similar until current index reaches 100, where the maximum fatigue damage of riser in case of 180 degree current direction is greater than case of 0 degree current direction.

For short-term fatigue damage calculation, the allowable maximum fatigue damage should be less than 1.0 over the period of each short-term event [37]. In both cases, the maximum fatigue damage is less than 1, which indicates the riser is safe from short-term fatigue damage. From the FD-CI diagram, the fatigue damage of steel catenary riser with outer diameter of 273.1mm can be estimated using the developed empirical equation, which maximum fatigue damage is

Near case (0 degree current heading direction)

$$FD = 2.641\times10^{-8}\cdot CI^{2} + 2.321\times10^{-7}\cdot CI + 1.081\times10^{-5} \tag{5.9}$$

Far case (180 degree current heading direction)

$$FD = 4.288\times10^{-8}\cdot CI^{2} + 1.509\times10^{-7}\cdot CI + 1.773\times10^{-5} \tag{5.10}$$

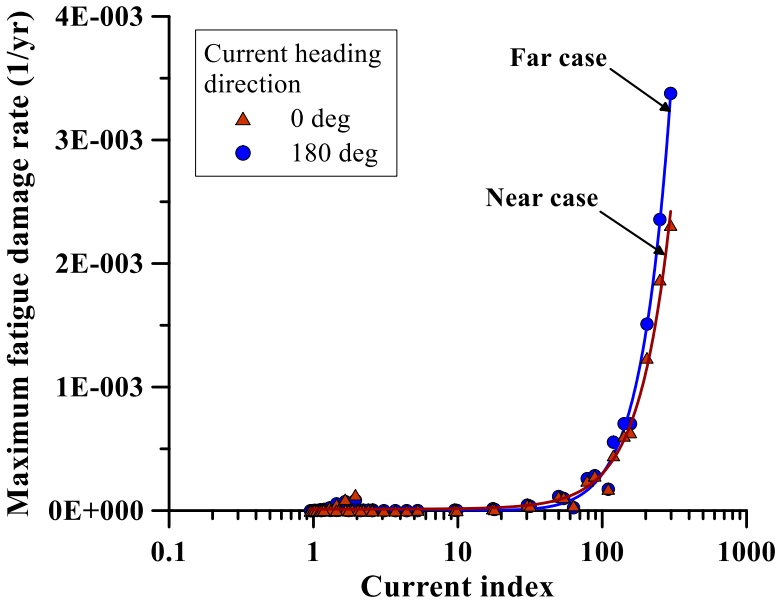

FIGURE 5.17: Comparison of fatigue damage for 0 and 180 degree current heading directions.

5.4.3 Comparison of Estimated Fatigue Damage Using Proposed Approach and SHEAR7

With the development of FD-CI diagram, the maximum fatigue damage of SCR can be estimated in shorter time using CI concept. The proposed approach for estimating the short-term VIV fatigue damage of SCR utilises the current index concept and FD-CI diagram. The approach is presented in the flowchart shown in Figure 5.18 below. To predict the maximum short term fatigue damage suffered by SCR due to VIV, first, using the given design current profile data provided in design basis or design data, the current index value can be calculated using the equation in Equation 5.7. By referring to FD-CI diagram, using the current index value calculated, the maximum fatigue damage of the SCR can be estimated with ease.

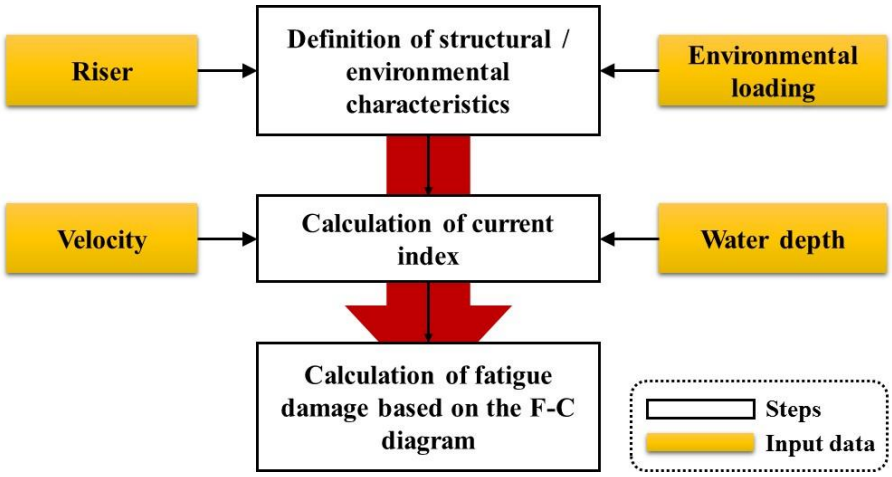

Figure 5.18: Flowchart of proposed approach for estimating short-term VIV fatigue damage using current index concept.

To validate the applicability of the proposed simplified VIV estimation approach, 6 current data from offshore development regions namely Brazil (Foz de Amazon), GOM, West Africa, Atlantic Frontier, and Northen Norway provided in Subsea Engineering Handbook [3] are used for estimation of VIV short term fatigue damage. The VIV fatigue damage of the SCR is calculated using the developed CI equation in Equation 5.7 and fatigue damage empirical equation in Equation 5.11 and 5.12. The calculated results were compared with the fatigue damage result computed using OrcaFlex and SHEAR7. Table 5.3 and Figure 5.19 and 5.20 show the comparison of the results.

TABLE 5.3: Comparison of maximum fatigue damage computed using proposed approach using CI concept and using industrial software, SHEAR7

No	Current Data Source	CI	Maximum Fatigue Damage using CI concept, FD_{CI} (1/yr)		Maximum Fatigue Damage using SHEAR7, FD_{SHEAR7} (1/yr)	
			Near Case	Far Case	Near Case	Far Case
1	Brazil (Foz de Amazon)	352.30	5.083E-03	3.551E-03	4.016E-03	2.429E-03
2	GOM (Hurricane)	0.76	1.699E-05	1.093E-05	1.037E-07	1.054E-07
3	GOM (Loop)	99.22	2.826E-04	2.879E-04	1.007E-04	9.942E-05
4	West Africa (Girassol)	13.62	5.188E-06	1.872E-05	2.467E-06	3.263E-06
5	Atlantic Frontier	112.27	6.665E-04	5.752E-04	1.854E-04	3.234E-03
6	Northern Norway	58.26	1.502E-04	1.806E-04	6.953E-05	9.316E-05

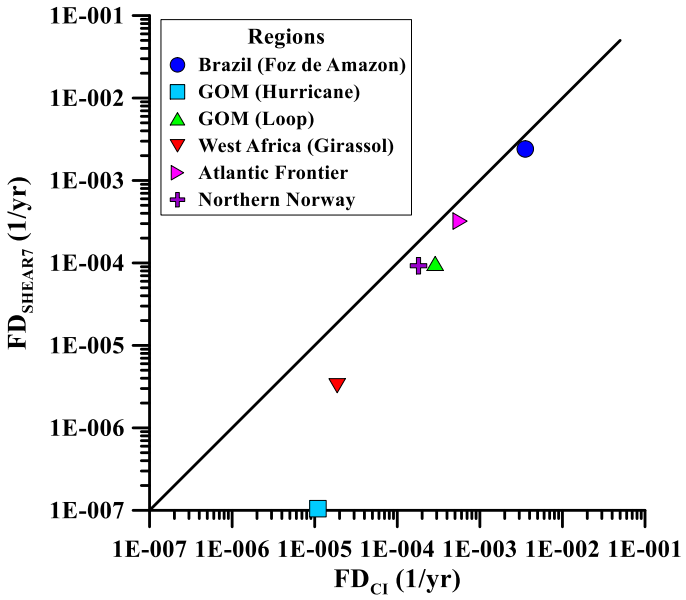

FIGURE 5.19: Comparison of maximum fatigue damage using proposed approach and SHEAR7 software for near case

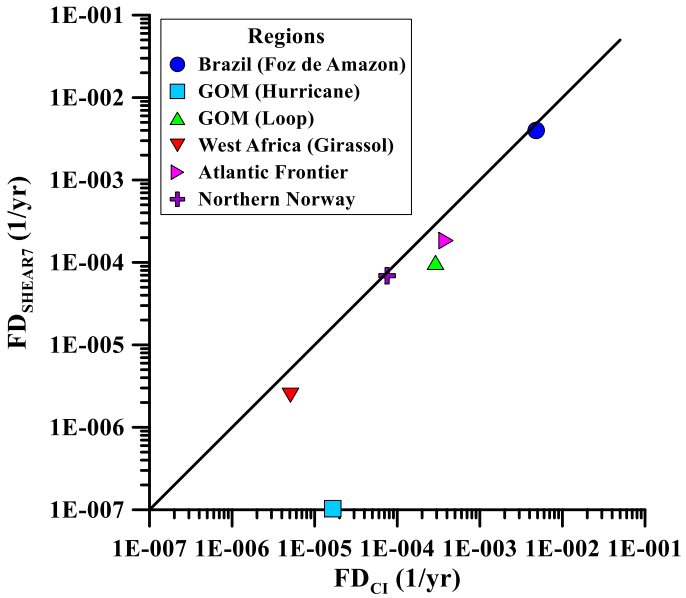

FIGURE 5.20: Comparison of maximum fatigue damage using proposed approach and SHEAR7 software for far case

The black line in Figure 5.19 and 5.20 is line of equality which indicates that the maximum fatigue damage calculated using proposed approach is equal to fatigue damage computed using SHEAR7. From Figure 5.19 and 5.20, it is observed that all the data points are in region below the black line, which implies the maximum fatigue damage estimated using CI concept is greater than maximum fatigue damage computed using SHEAR7. Most of the data points are closer to the line of equality, except for GOM (Hurricane), which shows a large difference from the result computed using SHEAR7. The calculated maximum fatigue damage using CI concept is much greater than using SHEAR7 software, proving that the result produced from CI concept is more conservative than result from software, indicating a higher safety factor. There is no data point that exist in upper region of the line of equality. This implies that the proposed approach provides more conservative results than estimations using SHEAR7.

Since CI concept is a simplified approach as compared to industrial VIV analysis software such as SHEAR7 and VIVANA, it produces estimated fatigue damage that is much more conservative than current practice using industrial software. Hence, it is more suitable to be used for screening purpose during concept generation stage instead of detailed VIV analysis purpose. This approach can be applied in PRE-FEED stage as screening purpose during the concept generation of feasible riser system for

potential offshore field development and production. It can ease decision making process for selecting suitable type of riser to be deployed for the specified environment condition when considering the potential short term VIV fatigue damage of SCR.

To improve the accuracy of the proposed CI concept and FD-CI diagram, future works such as incorporating different VIV parameter into the CI equation and taking into consideration of other environmental factors and riser structural properties, should be carried out consequently. Variation of current direction along the water depth should be investigated in future for better and more precise estimation of VIV fatigue damage of riser. Studies of other types of riser such top-tensioned riser (TTR), flexible riser and hybrid riser using the CI concept should be performed for the future work.

CHAPTER 6

CONCLUSION AND RECOMMENDATION

In this study, a new approach using current index concept is proposed for estimating short term fatigue damage of SCR caused by VIV. Compilation of current profile data and generation of statistical model of current profile variation with depth are performed using probability density distribution for preparation of current profile scenarios. Current index equation is developed and FD-CI diagrams are developed.

From the achieved outcomes, it is concluded that probability density distribution can be used to analyse the statistical properties of current profile to generate current profile model for preparation of design current data. From the VIV fatigue analysis of SCR, it is concluded that the maximum fatigue damage increases with current velocity. Hence, the relationship between the current velocity and maximum fatigue damage can be expressed in form of empirical equation, which maximum fatigue damage is proportional to current velocity raised to the power of 4.4. Current index equation, which is defined as function of current velocity, can be used to translate the current profile into characteristic value to be used to estimate fatigue damage of SCR. The relationship between the shear current profile and short-term VIV fatigue damage of SCR is established through the FD-CI diagram, which current index is used to convert the current profile into characteristic value. The relationship between maximum fatigue damage and current index can be summarised using empirical equation, such that maximum fatigue damage of SCR is expressed as polynomial function of current index. The proposed approach, using current index concept and FD-CI diagrams, produces result that is more conservative than current practice using industrial software. The proposed approach is expected to be able to be applied during preliminary design stage for the screening purpose for selection of suitable riser system to be employed in certain environmental condition to ease the process of estimating short term VIV fatigue damage.

It is recommended the variation in the direction of current to be investigated in future work in order to get more precise estimation of VIV fatigue damage. Effect of other VIV parameters and different riser structural properties to the VIV fatigue damage of SCR shall be performed. Study on the application of proposed approach in other types

of riser system such as TTR, flexible riser, attached riser and hybrid riser should be performed. Continuous validation and improvement shall be done to increase the accuracy and precision of the proposed approach. The output of the research is believed to enable easy prediction of VIV fatigue damage of SCR.

REFERENCES

[1] Y. Bai and Q. Bai, Subsea pipelines and riser, Elsevier Ltd., 2005.

[2] M. Duan, J. Chen and Z. Li, "Mechanics of Deepwater Steel Catenary Riser," in *Numerical Analysis - Theory and Application*, InTech, 2011.

[3] Y. Bai and Q. Bai, Subsea Engineering Handbook, Elsevier Inc., 2010.

[4] J. Brekke, S. Chakrabarti and J. Halkyard, "Drilling and production risers," in *Handbook of Offshore Engineering*, Elsevier Ltd., 2005.

[5] R. Bourguet, G. E. Karniadakis and M. S. Triantafyllou, "Lock-in of the vortex-induced vibrations of a long tensioned beam in shear flow," *Journal of Fluids and Structures*, vol. 27, pp. 838-847, 2010.

[6] A. D. Trim, H. Braaten, H. Lie and M. A. Tognarelli, "Experimental investigation of vortex-induced vibration of long marine risers," *Journal of Fluids and Structures*, vol. 21, pp. 335-361, 2005.

[7] S. Holmes, Y. Constantinides and O. W. Oakley, Jr., "Simulation of riser VIV using fully three dimensional CFD simulations," in *Proceedings of the 25th International Conference on Offshore Mechanics and Arctic Engineering*, 2006.

[8] S. Chen, "Fatigue damage prediction in deepwater marine risers due to vortex-induced vibration," Department of Civil Architectural and Environmental Engineering, University of Texas, 2011.

[9] D. W. Allen, "Vortex-induced vibration analysis of the Auger TLP production and steel catenary export risers," *Proceedings of Offshore Technology Conference*, 1995.

[10] Y. Gao, Z. Zong and L. Sun, "Numerical prediction of fatigue damage in steel catenary riser due to vortex-induced vibration," *Journal of Hydrodynamics*, vol. 23(2), pp. 154-163, 2011.

[11] M. Campbell, "The complexities of fatigue analysis for deepwater risers," in *Proceedings of Deepwater Pipeline Conference*, 1999.

[12] F. Lim and H. Howells, "eepwater riser VIV, fatigue, and monitoring," in *Proceedings of Deepwater Pipeline & Riser Technology Conference*, 2000.

[13] D. W. Allen and D. L. Henning, "Surface roughness effects on vortex-induced vibration of cylindrical structures at critical and supercritical Reynolds numbers," *Proceedings of Offshore Technology Conference*, 2001.

[14] R. D. Blevins, Flow-induced vibrations, Van Nostrand Reinhold Company, 2001.

[15] J. H. Lienhard, "Synopsis of lift, drag, and vortex frequency data for rigid circular cylinders," Washington State University, College of Engineering, Research Division Bulletin 300, 1966.

[16] J. K. Vandiver, "Dimensionless parameters important to the prediction of vortex-induced vibration of long, flexible cylinders in ocean currents," *Journal of Fluids and Structures,* vol. 7, pp. 423-455, 1993.

[17] J. K. Vandiver, D. W. Allen and L. Li, "The occurrence of lock-in under highly sheared conditions," *Journal of Fluids and Structures,* vol. 10, pp. 551-561, 1996.

[18] C. H. K. Williamson and R. Govardhan, "A brief review of recent results in vortex-induced vibrations," *Journal of Wind Engineering,* vol. 96, pp. 713-735, 2008.

[19] J. K. Vandiver and L. Li, "SHEAR7 v4.4 program theoretical manual," Massachusetts Institute of Technology, Department of Ocean Engineering, 2005.

[20] C. M. Larsen, K. Vikestad, R. Yttervik, E. Passano and G. S. Baarholm, "Theory Manual," MRINTEK 51310.01, 2000.

[21] M. S. Triantafyllou, "VIVA extended user's manual," Massachusetts Institute of Technology, Department of Ocean Engineering, 2003.

[22] K. W. Schulz and T. S. Meling, "VIV analysis of a riser subjected to step and multi-directional currents," in *Proceedings of ASME 2005 24th International Conference on Offshore Mechanics and Arctic Engineering*, 2005.

[23] R. H. J. Willden and J. M. R. Graham, "CFD simulations of the vortex-induced vibrations of model riser pipes," in *Proceedings of ASME 2005 24th International Conference on Offshore Mechanics and Arctic Engineering*, 2005.

[24] Z. M. Huang, "CFD simulation of riser VIV," Department of Ocean Engineering, Texas A&M University, 2011.

[25] J. R. Chaplin, P. W. Bearman, Y. Cheng, E. Fontaine, Craham, J. M. R., K. Herjford, Huarte, F. J. H., M. Isherwood, K. Lambrakos, C. M. Larsen, J. R. Meneghini, G. Moe, R. J. Pattenden, M. S. Triantafyllou and Willden, R. H. J., "Blind predictions of laboratory measurements of vortex-induced vibrations of a tension riser," *Journal of Fluids and Structures,* vol. 21, pp. 25-40, 2005.

[26] N. Srinil, M. Wiercigroch and P. O` Brien, "Reduced-order modelling of vortex-induced vibration of catenary riser," *Ocean Engineering,* vol. 36, pp. 1404-1414, 2009.

[27] Y. Gao, Z. Zong, L. Zhou and J. Cao, "Analysis of vortex induced vibration fatigue damage of steel catenary riser," *Chinese Journal of Ship Research,* vol. 5(5), pp. 54-63, 2010.

[28] E. Lejlic, "Vortex induced fatigue damage of a steel catenary riser near the touchdown point," Department of Marine Technology, Norwegian University of Science and Technology, 2013.

[29] L. M. Quéau, M. Kimiaei and M. F. Randolph, "Artificial neural network development for stress analysis of steel catenary risers: Sensitivity study and approximation of static stress range," *Applied Ocean Researc,* vol. 48, pp. 148-161, 2014.

[30] L. Sun, C. F. Liu, Z. Zong and X. L. Dong, "Fatigue damage analysis of the deepwater riser from VIV using pseudo-excitation method," *Marine Structures,* vol. 37, pp. 86-110, 2014.

[31] K. P. Wang, W. Y. Tang and H. X. Xue, "Time domain approach for coupled cross-flow and in-line VIV induced fatigue damage of steel catenary riser at touchdown zone," *Marine Structures*, vol. 41, pp. 267-287, 2015.

[32] K. S. Park, "Fatigue Performance of Deepwater Steel Catenary Riser," M.Sc. dissertation, Graduate School of Engineering Mastership, Pohang University of Science and Technology, Pohang, South Korea, 2014.

[33] Orcina Ltd., "OrcaFlex manual," 2014.

[34] T. W. Anderson and D. A. Darling, "A test of goodness-of-fit," *Journal of the American Statistical Association*, 1994.

[35] D W. Scott, *Multivariate Density Estimation: Theory, Practice, and Visualization*. New York: John Wiley, 1992.

[36] American Petroleum Institute (API), *Design of risers for floating production systems (FPSs) and tension-leg platforms (TLPs)*. Recommended Practice 2RD, 1998.

[37] Det Norske Veritas (DNV), *Riser Fatigue*. Recommended Practice F204, 2010.

APPENDICES

APPENDIX A: SCR MODEL INPUT DATA

1. SCR pipe structural data

TABLE A1: SCR pipe structural data [32]

Parameter		**Production SCR**
		10 in
Dimensions		
Outer diameter (mm)		273.1
Wall thickness (mm)		30.0
Internal corrosion allowances (mm)		1.59
External corrosion allowances (mm)		None
Material properties		
Material		API X-65 Steel
Density (kg/m^3)		7849
Minimum yield strength (MPa)		448
Young's modulus (MPa)		208774
Shear modulus (MPa)		78759
Tangent modulus (MPa)		457
Poisson ratio		0.3
Anti-corrosion coating		
Straked/Bare pipe region		
FBE coating	**Thickness (mm)**	0.559
	Density (kg/m^3)	1442
Touchdown zone region		
TLPE	**Thickness (mm)**	3.175
	Density (kg/m^3)	961

2. Internal fluid data

TABLE A2: Internal fluid data [32]

Parameter		**Value**
Production SCR	Condition	Shut-in
	Pressure (kPa)	50193.8
	Density (kg/m^3)	310.8

3. Tapered stress joint properties

TABLE A3: SCR Tapered stress joint properties [32]

Parameter	**SCR**
	10 in
Material	Titanium
Minimum yield strength (MPa)	758
Young's modulus (MPa)	115.14
Density (kg/m^3)	4509
Poisson ratio	0.33
Total length (m)	6.644
Tapered section	
L_1 (m)	3.753
OD_1 (m)	0.315
ID_1 (m)	0.213
OD_2 (m)	0.273
ID_2 (m)	0.213
Straight section	
L_2 (m)	2.892
OD (m)	0.273
ID (m)	0.213

4. Strake properties

TABLE A4: SCR Strake properties [32]

Parameter	**SCR**
	10 in
Density (kg/m^3)	1150.82
Section weight in air (kg/m)	39.51
Section weight in water (kg/m)	4.29
Barrel outside diameter (mm)	334.16
Barrel thickness (mm)	30.00
Equivalent thickness for $D_{hydrodynamic}$ (mm)	5.07
Strake height (0.25D) (mm)	83.54
Strake pitch (16D) (mm)	5346.60

5. Associated wave and wind data

TABLE A5: Associated wave and wind data [32]

Return Period (yr)	**1**
Waves, WD >= 1000 m	
Significant wave height (Hs, m)	2.1
Peak spectral period (Tp, s)	6.8
Peak enhancement factor (g)	2.4
Wind at 10m elevation (NPD)	
1 hr mean wind speed (m/s)	9.7

6. Soil friction coefficient and stiffness

TABLE A6: Soil friction coefficient and stiffness [32]

Parameters	**Value**
Normal seabed friction coefficient	1.0
Axial seabed friction coefficient	0.5
Normal seabed stiffness (kN/m/m^2)	115
Shear seabed stiffness (kN/m/m^2)	79

7. Soil friction coefficient and stiffness

Equation of the S-N curve is defined as below and parameters for S-N curve is defined in Table A7.

$$\Delta\sigma = \left(\frac{10^a}{N}\right)^{\frac{1}{b}} \tag{A.1}$$

TABLE A7: S-N curve parameter [32]

S-N curve	**Intercept (a)**	**Slope of curve (b)**
RITES (TSJ)	37.832	6
DNV C (SCR)	12.192	3

APPENDIX B: GANTT CHART AND MILESTONES

Gantt Chart

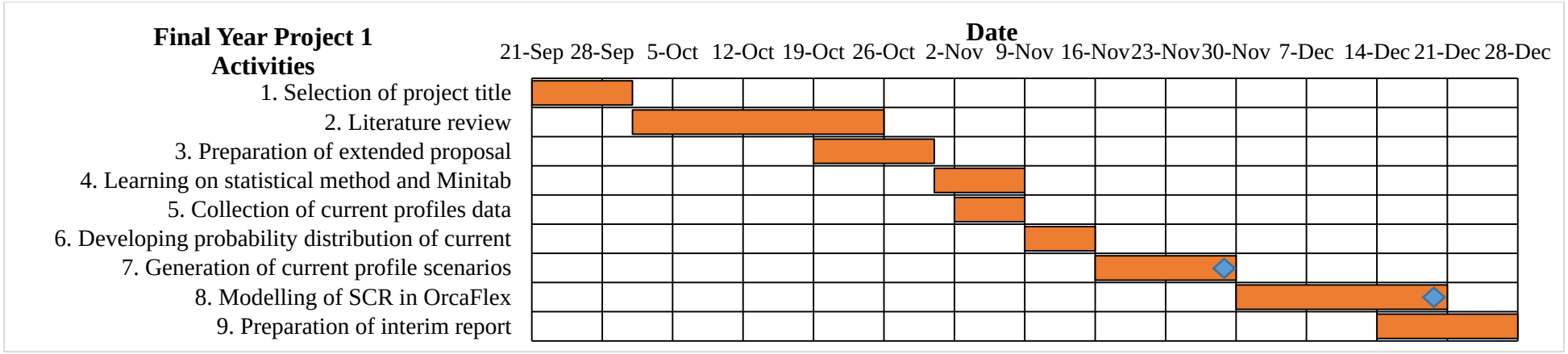

FIGURE B.1: Gantt chart for Final Year Project 1

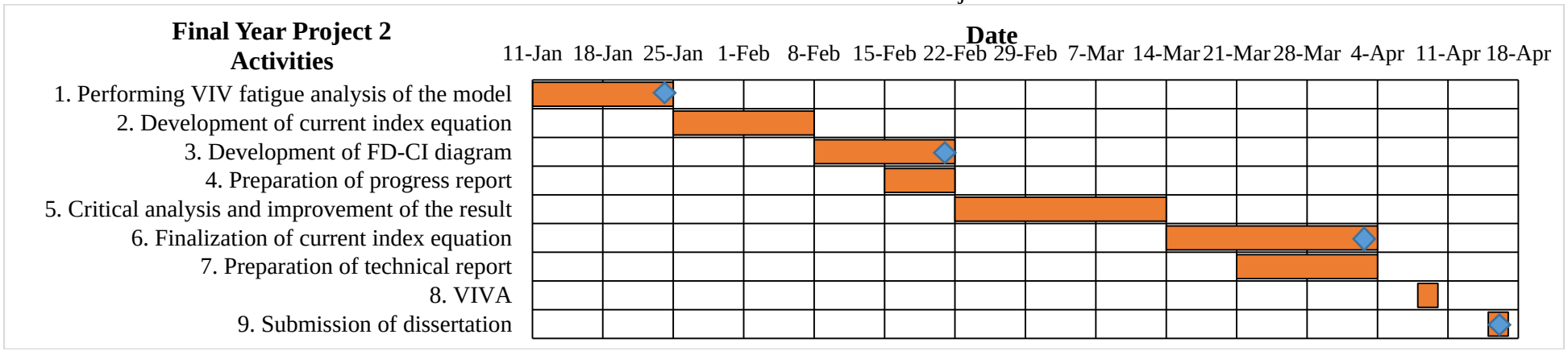

FIGURE B.2: Gantt chart for Final Year Project 2

Key Milestones

No.	Week	Key Milestone
1	Week 6 (FYP1)	Submission of extended proposal.
2	Week 11 (FYP1)	Completion of generation of current profile model by statistical mean.
3	Week 13 (FYP1)	Completion of SCR modelling.
4	Week 14 (FYP1)	Submission of interim report.
5	Week 2 (FYP2)	Completion of VIV fatigue analysis of SCR model.
6	Week 6 (FYP2)	- Completion of development of FD-CI diagrams. - Submission of progress report.
7	Week 12 (FYP2)	- Finalization of current index equation and FD-CI diagrams - Submission of technical report.
8	Week 13 (FYP2)	VIVA presentation.
9	Week 14 (FYP2)	Submission of dissertation.

APPENDIX C: BEST FIT PROBABILITY DENSITY DISTRIBUTION FOR EACH NORMALIZED WATER DEPTH

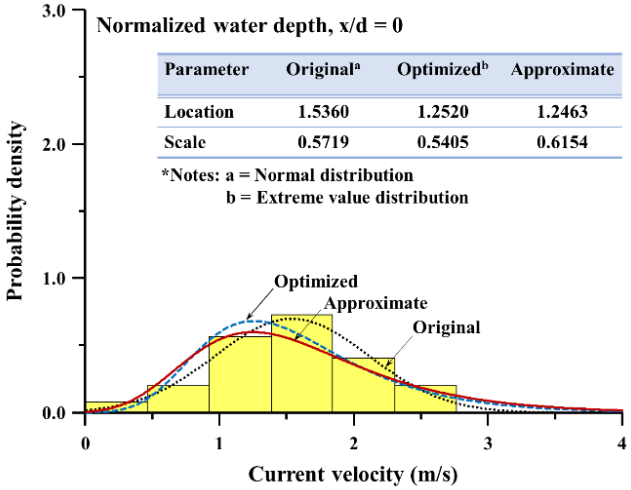

(a) Current velocity at x/d = 0

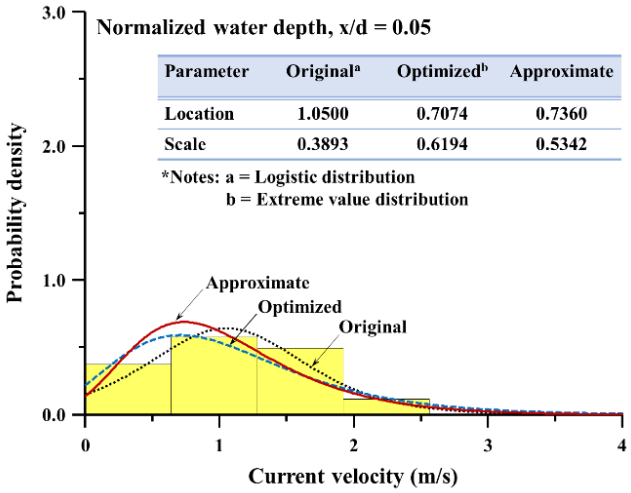

(b) Current velocity at x/d = 0.05

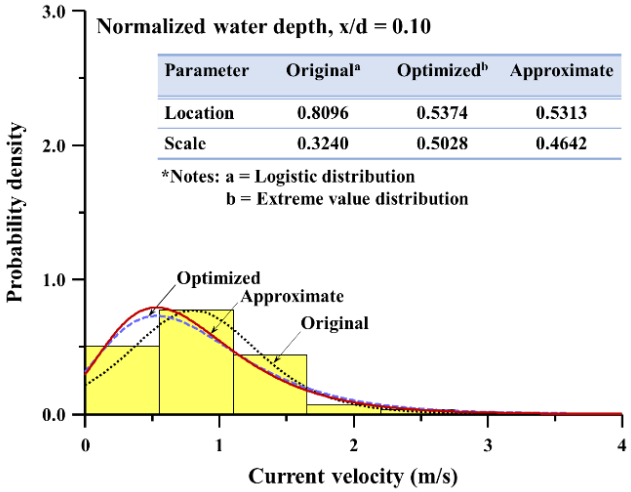

(c) Current velocity at x/d = 0.10

FIGURE C.1: Best fit probability density distribution for each normalized water depth

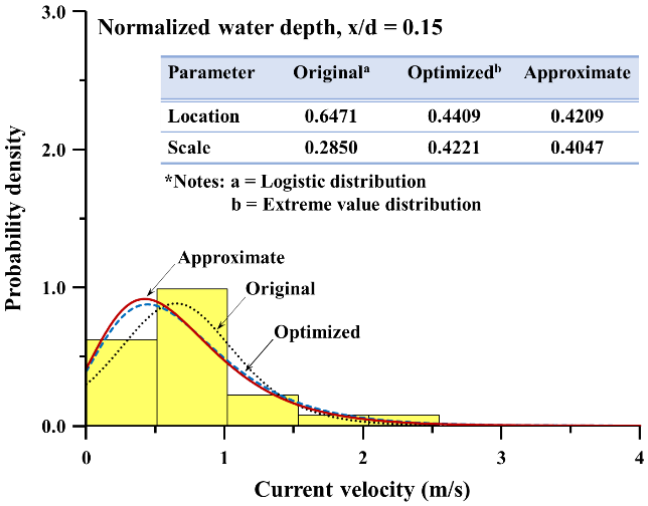

(a) Current velocity at x/d = 0.15

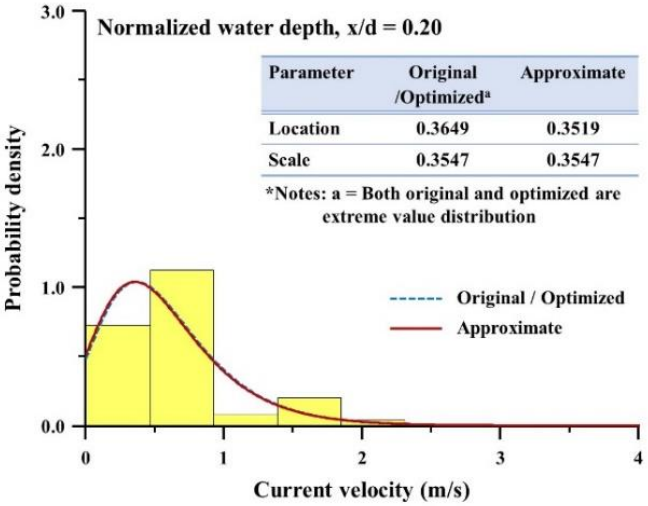

(b) Current velocity at x/d = 0.20

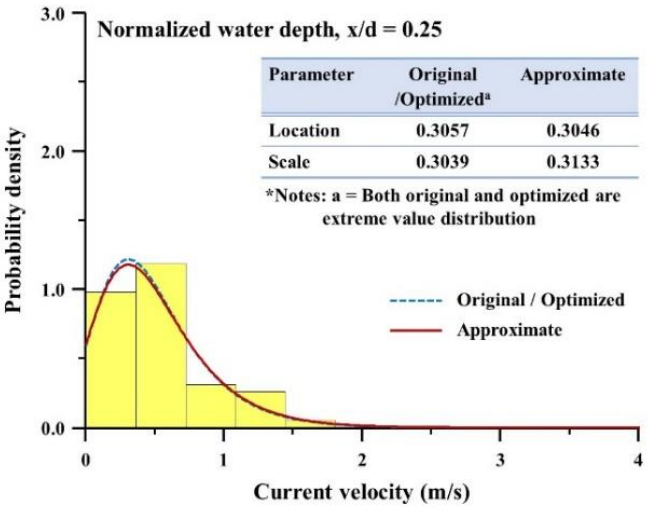

(c) Current velocity at x/d = 0.25

FIGURE C.2: Best fit probability density distribution for each normalized water depth

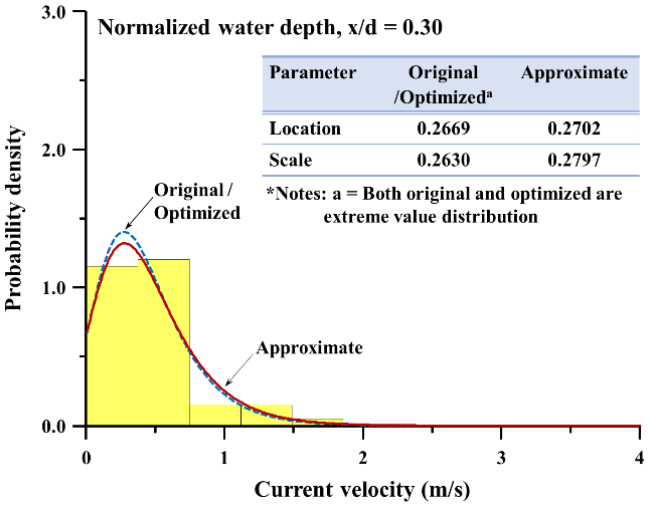

(a) Current velocity at x/d = 0.30

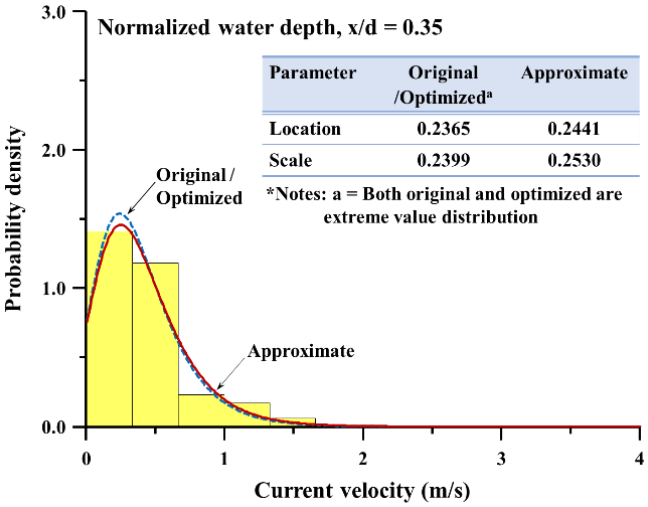

(b) Current velocity at x/d = 0.35

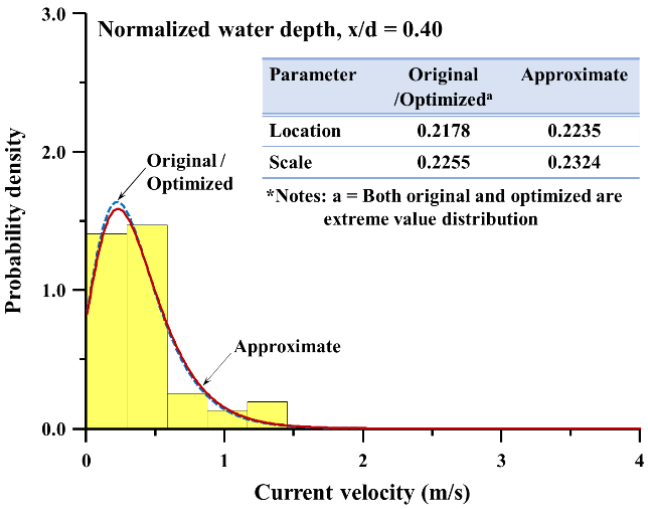

(c) Current velocity at x/d = 0.40

FIGURE C.3: Best fit probability density distribution for each normalized water depth

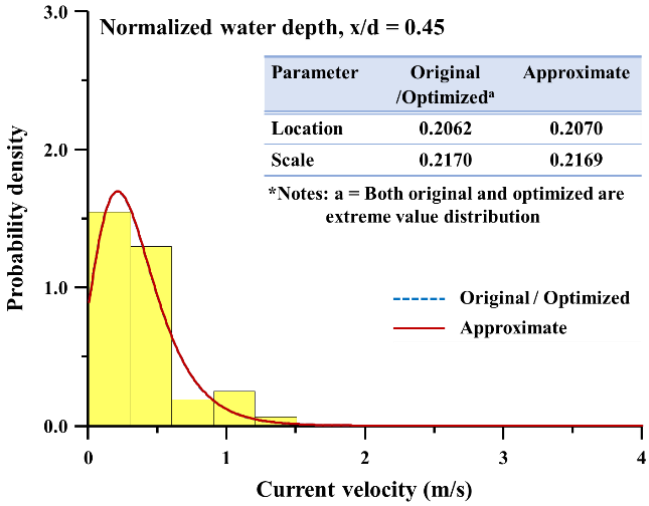

(a) Current velocity at x/d = 0.45

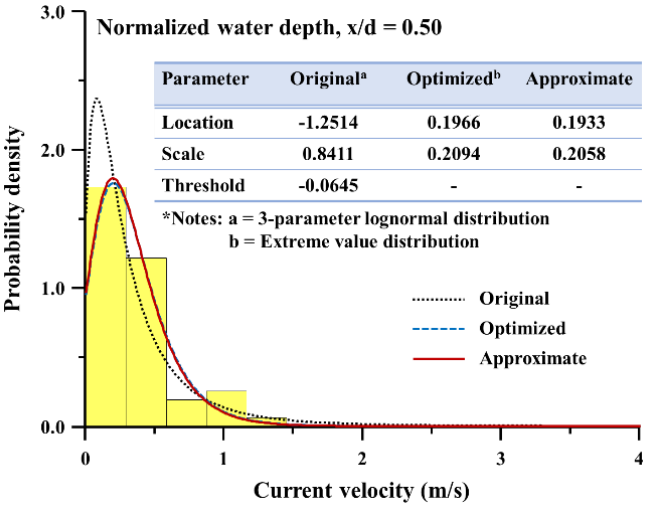

(b) Current velocity at x/d = 0.50

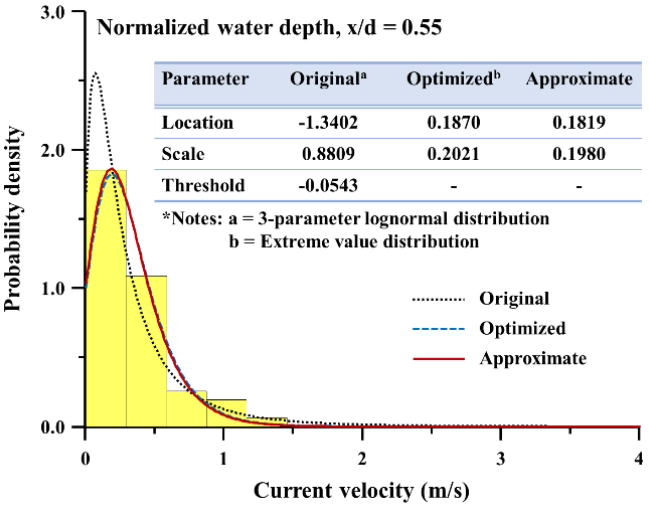

(c) Current velocity at x/d = 0.55

FIGURE C.4: Best fit probability density distribution for each normalized water depth

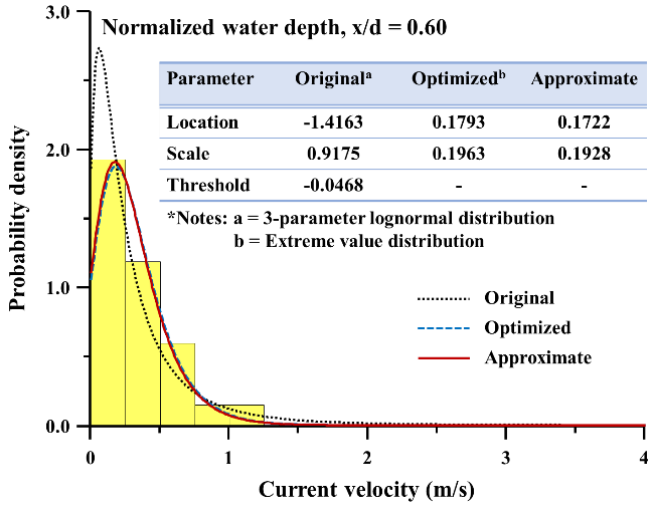

(a) Current velocity at x/d = 0.60

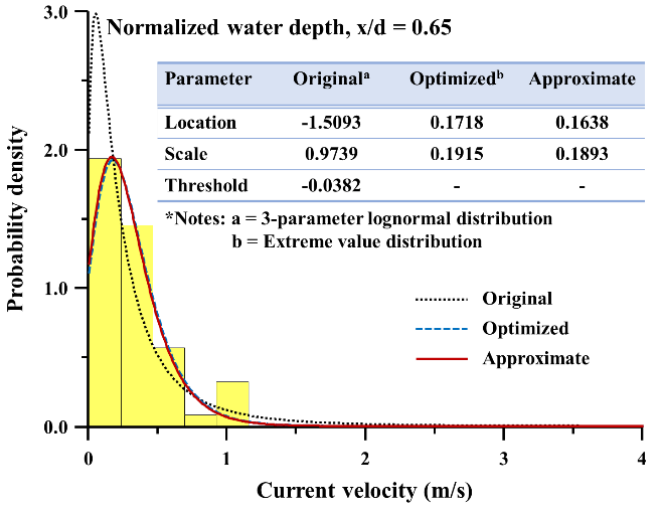

(b) Current velocity at x/d = 0.65

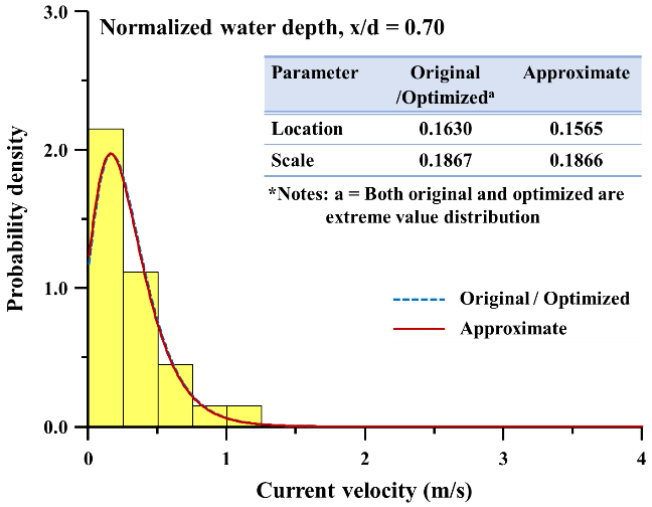

(c) Current velocity at x/d = 0.70

FIGURE C.5: Best fit probability density distribution for each normalized water depth

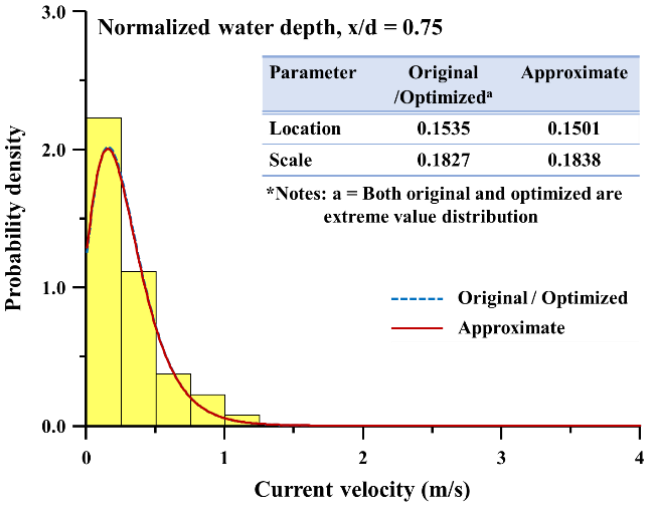

(a) Current velocity at x/d = 0.75

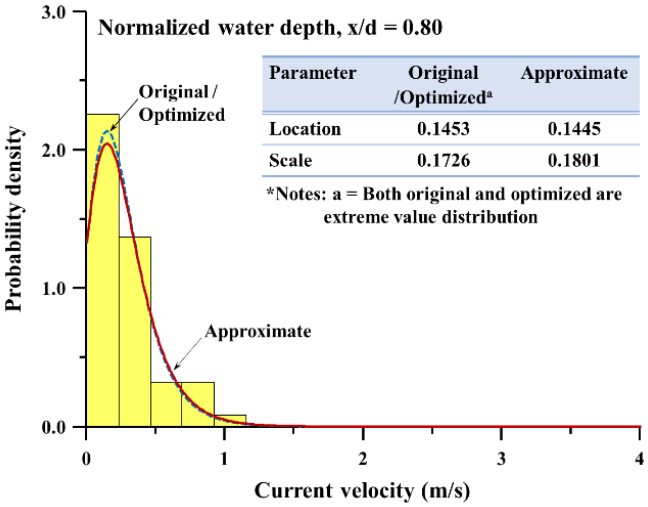

(b) Current velocity at x/d = 0.80

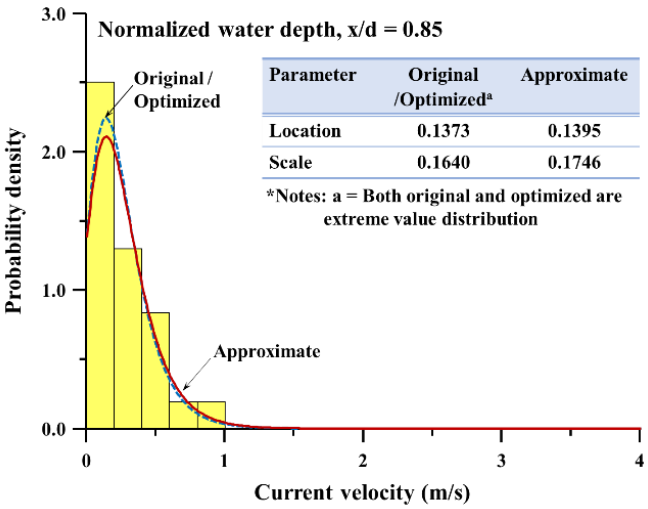

(c) Current velocity at x/d = 0.85

FIGURE C.6.: Best fit probability density distribution for each normalized water depth

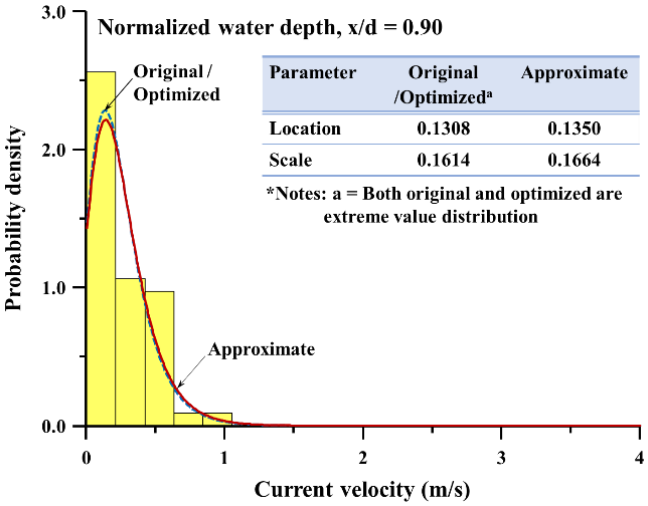

Parameter	Original /Optimized[a]	Approximate
Location	0.1308	0.1350
Scale	0.1614	0.1664

*Notes: a = Both original and optimized are extreme value distribution

(a) Current velocity at x/d = 0.90

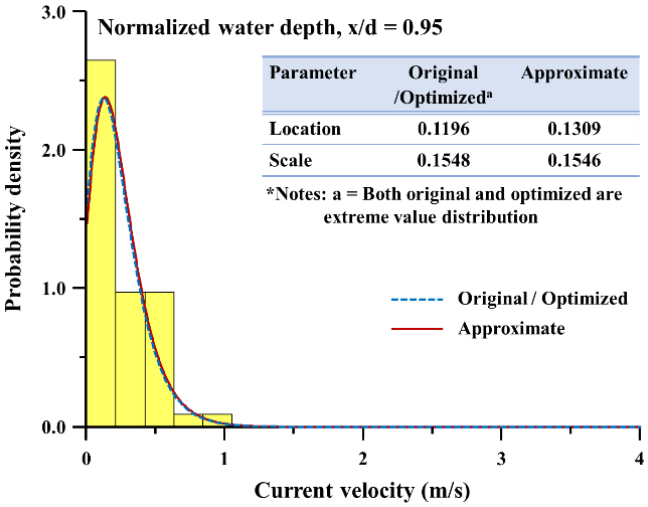

Parameter	Original /Optimized[a]	Approximate
Location	0.1196	0.1309
Scale	0.1548	0.1546

*Notes: a = Both original and optimized are extreme value distribution

(b) Current velocity at x/d = 0.95

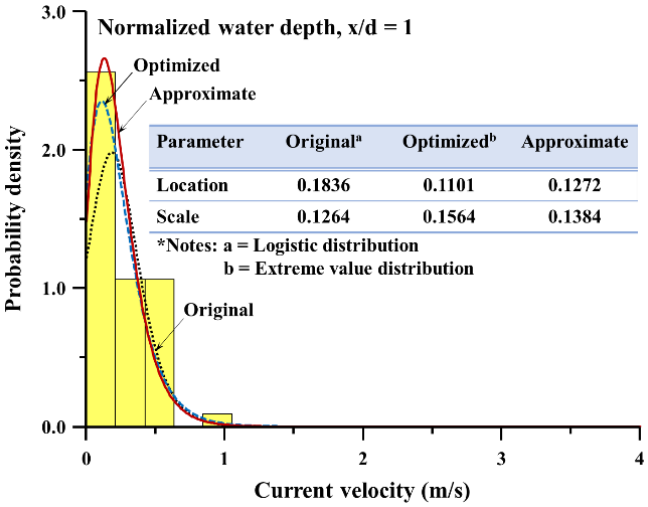

Parameter	Original[a]	Optimized[b]	Approximate
Location	0.1836	0.1101	0.1272
Scale	0.1264	0.1564	0.1384

*Notes: a = Logistic distribution
b = Extreme value distribution

(b) Current velocity at x/d = 1

FIGURE C.7: Best fit probability density distribution for each normalized water depth